SOILS AND FOUNDATIONS Vol. 44, No. 1, 125–142, Feb. 2004
Japanese Geotechnical Society

NUMERICAL METHOD FOR CONSOLIDATION ANALYSIS OF LUMPY CLAY FILLINGS WITH MESHLESS METHOD

TOYOAKI NOGAMI[i], W. WANG[ii] and J. G. WANG[iii]

ABSTRACT

A numerical method is developed for consolidation analysis of lumpy clay fillings by using the double porosity model and the meshless method. Lumpy clay fillings consist of inter-lump voids and a clay matrix, which further consists of soil frame and pores. When a load is applied to these fillings submerged in the water, pore water pressures are generated and dissipate in the inter-lump voids and matrix. The model accounts for the coupling between the deformation of the soil skeleton and the excess pore water pressures in both the matrix and inter-lump voids, and also the fluid exchange between the inter-lump voids and matrix. The meshless method based on the radial point interpolation method (radial PIM) is used for spatial discretizations of displacement and pore water pressures. The order of interpolation function for the displacement is one order higher than that for pore water pressure to improve the numerical problem. Time domain is discretized through the backward Euler algorithm. The developed method is verified through a benchmark problem and two centrifuge tests. Finally, the effects of variations of various key parameters on the consolidation process are numerically studied for one-dimensional and plane strain (two-dimensional) problems. It is found that the developed numerical approach can successfully simulate the consolidation behavior of lumpy clay fillings despite their complex behaviour.

Key words: consolidation, double porosity medium, lumpy clay, meshless method, radial point interpolation (**IGC**: E2/E7/E13)

INTRODUCTION

Land reclamation has been a common practice for creating valuable land in civil engineering. Two kinds of filling methods have been used for land reclamation with dredged clay. The first method is hydraulic fillings, where hydraulic force is used to transport and place fills. The soils are fluidized or muddy in this method. Fills placed in this manner are fairly homogeneous and idealized as a porous medium with relatively uniform pores. Conventional consolidation theories are applicable for such fills. A cramp bucket is also used for dredging seabed soils. In such dredging, stiff clay scooped from the seabed forms a lump. The second filling method is to directly dump these clay lumps into the reclamation site as a fill material. This not only solves the disposal problem of dredged soils but also saves land reclamation costs. One of the earliest dumping filling projects was reported in Halmstad Harbor in Sweden (Hartlen and Inters, 1981). Since the 1980's, several reclamation projects have been completed or are in progress in Singapore with lumpy fillings (Ganesan, 1998; Leung et al., 1996, 2001; Wong, 1997).

Lumpy clay fillings are a dual porosity system: a macro-system is made of lumps and inter-lump voids, while a micro-system is made of the clay matrix in an individual lump. The behaviors of pore water pressure dissipations in inter-lump voids and the clay matrix are quite different from each other. This is attributed to the distinctly different permeability and compressibility between the clay matrix and inter-lump structure. Adding further complexity, inter-lump voids may be closed-up with loading. In order to investigate such complex geotechnical characteristics of lumpy clay, centrifuge and one-dimensional laboratory tests were conducted at the National University of Singapore. For examples, Leung et al. (1996, 2001) used prototype dredged clay lumps in their tests, while Manivannan (1999) used different reduced sizes in centrifuge tests. Consolidation and deformation characteristics of lumpy clay fillings were observed physically in these tests.

Numerical simulation of the consolidation process of lumpy clays is quite complicated because of strong heterogeneity in their structures, which results from coexistence of micro and macro porous systems which are mutually distinct. Conventional consolidation theories such as Terzaghi's or Biot's consolidation theory are not applicable for such soils. Up to date, only a few numerical simulations have been tried to describe the

[i] Professor, Dept. of Civil Engineering, National University of Singapore, Singapore 117576 (toyoakinogami@yahoo.com).
[ii] Research Scholar, ditto.
[iii] Research Fellow, ditto.
Manuscript was received for review on November 21, 2002.
Written discussions on this paper should be submitted before September 1, 2004 to the Japanese Geotechnical Society, Sugayama Bldg. 4F, Kanda Awaji-cho 2-23, Chiyoda-ku, Tokyo 101-0063, Japan. Upon request the closing date may be extended one month.

consolidation characteristics of lumpy fillings. Wang et al. (1997) proposed a homogenization method to formulate the heterogeneous consolidation behaviors of dredged lumpy clays. It is based on the Terzaghi-Rendulic consolidation theory that does not include the deformation of the macro-system, in which the physical properties of the clay matrix and inter-lumpy voids are considered separately. The double porosity concept is a quite effective approach to analyze the behavior of a fissured porous media, mainly used in petroleum and water resources engineering (Elsworth and Bai, 1992; Berryman and Wang, 1995; Bai et al., 1994; Bai and Roegiers, 1994; Ghafouri and Lewis, 1996; Valliappan and Khalili, 1990). Nogami et al. (2001) applied this double porosity concept model to the consolidation analysis of lumpy clays for the first time. They developed a matrix transfer method for its numerical solution. In their solution, only a one-dimensional condition was considered for consolidation of lumpy clay fillings and thus a constant total stress was assumed during the whole consolidation process. However, applicability of the double porosity model was examined to only a limited extent in their study.

Mesh-dependency methods such as the Boundary Element Method (BEM) and Finite Element Method (FEM) are powerful means to solve the coupled soil consolidation problems. However, both BEM and FEM are mesh-based methods, which require a pre-defined connectivity for all the elements. As a result, the generation of suitable meshes for the problem domain can take most of the computational time and effort, rather than solving the governing partial differential equations themselves. And it is widely acknowledged that mesh generation remains one of the biggest challenges in mesh-based methods

To avoid the difficulties arising from mesh generation, considerable efforts have been devoted to the development of a so-called meshless method. It abandons the element concept for constructing approximation functions for field variables and only uses a set of nodes to discretize the problem domain. There is no fixed connectivity among nodes and hence it can remove or at least alleviate the difficulty of meshing and re-meshing the problem domain by simply adding or deleting nodes.

The initial idea of meshless methods dates back to the smooth particle hydrodynamics (SPH) methods for modeling astrophysical phenomena (Lucy, 1977). Since then, the research into meshless methods has achieved remarkable progress and these have been reported in literatures, such as Diffuse Element Method (DEM) (Nayroles et al., 1992), Element-Free Galerkin Method (EFGM) (Belytschko et al., 1994), Reproducing Kernel Particle Method (RKPM) (Liu et al., 1995), h-p clouds (Duarte and Oden, 1996), the Partition of Unity (Babuska and Melenk, 1997) etc.

Modaressi et al. (1996) first adopted the meshless concept to develop a mixed DEM-FEM approach for a transient coupled analysis for consolidation of soil, where the displacement of the soil skeleton is modeled by standard finite elements and the pore water pressure by element free nodes. After that, Modaressi et al. (1998) solved the problem of analyzing consolidation of three-phase porous medium by applying the mixed EFGM-FEM approach. Nogami and his co-workers (2001) adopted EFGM to solve Biot's consolidation equations for a wide range of engineering problems. In addition, EFGM was also adopted by Murakami et al. (2001) to analyze the behavior of saturated soil. All of the above meshless approaches to solve Biot's consolidation equations share the same essential characteristics in that they are all based on moving least-square (MLS) approximations and their interpolation shape functions are polynomials associated with nodal values by weighted least-squares approximations.

Unlike other meshless methods employing the MLS, the basic idea of point interpolation method (PIM) is to provide an interpolation method through a data point, so that the enforcement of essential boundary conditions may be simplified. The basis used in PIM is polynomials. The order of polynomials is dependent on the number of nodes which contribute to the approximation. It has its shape functions with Kronecker delta properties and only one inverse matrix to obtain its shape function and derivatives. Wang et al. (2001) adopted this method for the transient coupled field analysis of soil consolidation and obtained satisfactory results.

However, PIM is not without shortcomings. The main drawback of PIM is that singular matrices may occur if the arrangement of a set of scattered nodes is not consistent with the order of basis. In order to overcome this difficulty, a point interpolation meshless method based on radial basis functions (radial PIM) was proposed by Wang and Liu (2002). The most attractive characteristic of the radial PIM is that singularity can be successfully avoided for arbitrarily scattered nodes by adopting the radial and polynomial basis function together. Wang et al. (2002) applied it to solve the Biot's consolidation equations and obtained satisfying results. However, because the radial PIM meshless method still depends on the background meshes to perform the integration, it is regarded as a pseudo-meshless method.

This paper developed a numerical method for consolidation analysis of lumpy clay fillings, adopting the double porosity model and the meshless method based on the radial point interpolation method. First, consolidation equations are presented for lumpy clay fillings by using the double porosity model. These equations are discritised with the radial PIM, specially formulated with the interpolation functions of mutually different order for displacement and pore water pressures. The developed method and computer code are verified by using other numerical methods and centrifuge test results. Finally, the consolidation characteristics of lumpy fillings are studied through parameter studies.

GOVERNING EQUATIONS

Lumpy clay fillings consist of randomly distributed lumps as a macro-system and the clay matrix in an

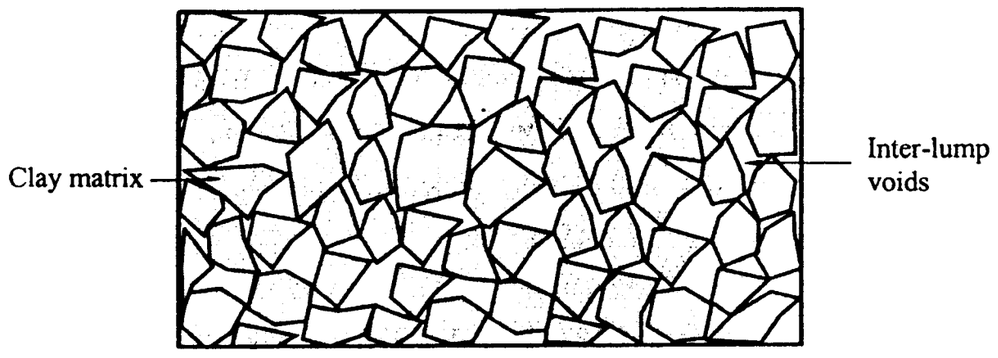

Fig. 1. Typical lumpy clay fillings

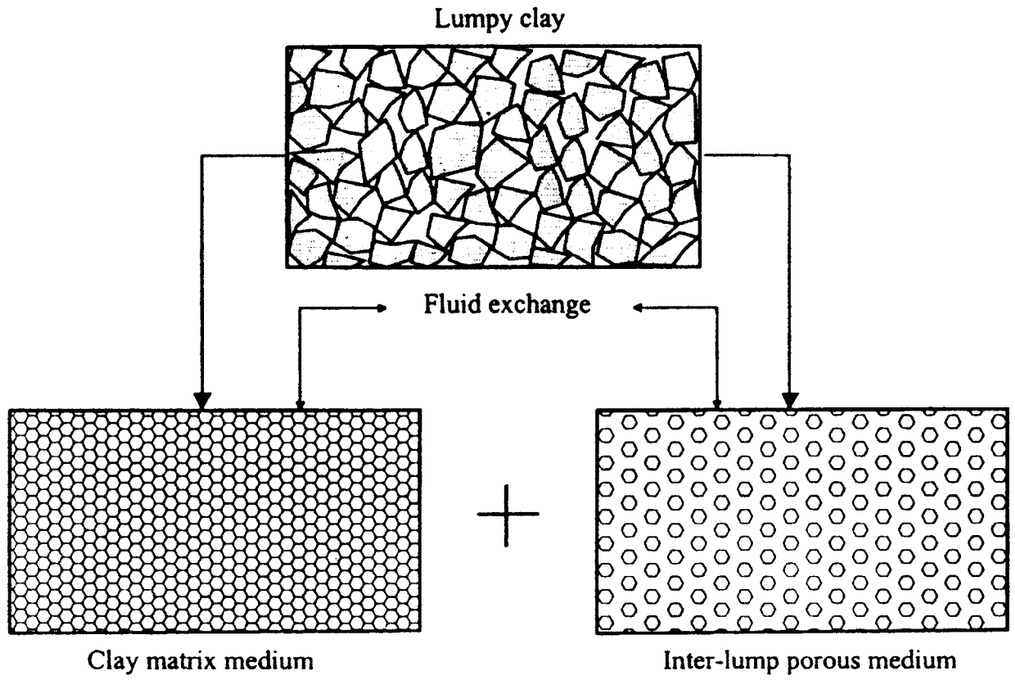

Fig. 2. Representation of lumpy clay fillings through double porosity model

individual lump as a micro-system as shown in Fig. 1. When an external load is applied to the fillings, pore water pressure is generated not only within inter-lump voids but also within matrix pores. As a result, the fluid exchange takes place between the two domains as the fluid in inter-lump voids is squeezed out. Although the pore fluids in matrix pores and inter-lump voids occupy different spaces, this process is formulated assuming that a homogeneous quantity of each in the two domains is distributed uniformly over the lumpy clay space as shown in Fig. 2. According to such a treatment, two pore water pressures are defined at each spatial point. This "two-pressure at one point" scenario is a convenient treatment often used in the computational field. Soil particles and pore fluid are assumed to be incompressible.

For comprehensive presentation, the consolidation equations for the double porosity medium are briefly presented. Details can be found in references (Khalili and Valliappan, 1995; Wilson and Aifantis, 1982; Lewallen and Wang, 1998). Scripts 1 and 2 in the formulations presented below denote respectively the clay matrix (micro-system) and the inter-lump frame structure (macro-system) of lumpy clay fillings.

Deformation Equations

A volume of lumpy clay fillings as shown in Figs. 1 and 2 is considered. Its equilibrium equation is expressed with the total stress (σ_{ij}^0) and body force per unit volume (b_i) as

$$(\sigma_{ij}^0)_{,j} + b_i = 0 \tag{1}$$

In this paper, $(\dot{*}) = \partial(*)/\partial t$, $(\dot{*})_{,i} = \partial^2(*)/\partial x_i \partial t$ and $(*)_{,i} = \partial(*)/\partial x_i$ are defined; and index summation is implicit.

An equivalent effective stress law for double porosity media can be obtained by using a single effective stress law (Nur and Byerlee, 1971), expressed as

$$\sigma_{ij}^0 = \sigma_{ij} + \delta_{(1)} p_{(1)} \delta_{ij} + \delta_{(2)} p_{(2)} \delta_{ij} \tag{2}$$

where δ_{ij} is Kronecker's delta; σ_{ij} denotes the equivalent effective stress for double porous media; $p_{(1)}$ and $p_{(2)}$ denote pore water pressures in clay matrix and inter-lump voids, respectively; and $\delta_{(1)}$ and $\delta_{(2)}$ are defined as (Li, 2001)

$$\delta_{(1)} = \frac{m_c}{m}, \quad \delta_{(2)} = 1 - \frac{m_c}{m} \tag{3}$$

with the compressibility of matrix (m_c) and the overall or macro volumetric compressibility of lump clay fillings (m). For linearly elastic medium, m is expressed with Poisson's ratio υ and Young's modulus E:

$$m = \frac{(1-2\upsilon)(1+\upsilon)}{(1-\upsilon)E} \quad \text{in the one-dimensional condition} \tag{4a}$$

$$m = \frac{2(1-2\upsilon)(1+\upsilon)}{E} \quad \text{in the two-dimensional condition} \tag{4b}$$

Increments of volumetric strains are expressed as (Li, 2001)

$$d\varepsilon_{v(1)} = \delta_{(1)} d\varepsilon_v - m_c(\delta_{(2)} - n_{(2)}) dp_{(1)} + m_c(\delta_{(2)} - n_{(2)}) dp_{(2)} \tag{5a}$$

$$d\varepsilon_{v(2)} = \delta_{(2)} d\varepsilon_v + m_c(\delta_{(2)} - n_{(2)}) dp_{(1)} - m_c(\delta_{(2)} - n_{(2)}) dp_{(2)} \tag{5b}$$

where "d" expresses the increment; $n_{(2)}$ is the porosity of inter-lump porous medium; and $\varepsilon_{v(1)}$, $\varepsilon_{v(2)}$ and ε_v are respectively the volumetric strains of clay matrix, inter-lump frame structure and overall system. ε_v is expressed as

$$\varepsilon_v = \frac{\partial u_i}{\partial x_i} \tag{6}$$

In this paper, the double porosity formulation is used for consolidation of lumpy clay fillings. The development of formulation is based on the linear elastic condition. Such formulation can be justified since the linear elastic soil is generally used in practice in the predication of pore water pressure dissipation. By using an appropriate non-linear constitutive law, it can also be extended for non-linear analysis. Hooke's law and equivalent strain ε_{ij} for lumpy clay fillings can be written respectively as

$$\sigma_{ij} = 2G\varepsilon_{ij} + \lambda \varepsilon_{kk} \delta_{ij} \tag{7a}$$

$$\varepsilon_{ij} = \frac{1}{2}\left(\frac{\partial u_i}{\partial x_j} + \frac{\partial u_j}{\partial x_i}\right) \tag{7b}$$

where G and λ are Lame's constants.

From Eqs. (1) through (7), the Navier equation for lumpy clay fillings is obtained as

$$G\frac{\partial^2 u_i}{\partial x_j \partial x_j}+(\lambda+G)\frac{\partial^2 u_j}{\partial x_j \partial x_i}+\delta_{(1)}\frac{\partial p_{(1)}}{\partial x_i}+\delta_{(2)}\frac{\partial p_{(2)}}{\partial x_i}+b_i=0. \quad (8)$$

Flow Equations

Darcy's law is assumed for seepage flow in either clay matrix or inter-lump voids, namely

$$q_{i(\alpha)}=-\frac{k_{ij(\alpha)}}{\gamma_w}\frac{\partial p_{(\alpha)}}{\partial x_j} \quad (9)$$

where $q_{i(\alpha)}$, $k_{ij(\alpha)}$ and $p_{(\alpha)}$ are respectively the discharge of fluid, permeability and excess pore water pressure; indices α denotes clay matrix ($\alpha=1$) or inter-lump porous media ($\alpha=2$); and i and j denote the x-coordinate (i and $j=1$) or z-coordinate (i and $j=2$). A rate of fluid exchange between the matrix and inter-lump voids, $q_{(\alpha)}$, is assumed to be proportional to their pressure difference, expressed as

$$q_{(\alpha)}=(-1)^{\alpha}\gamma(p_{(1)}-p_{(2)}) \quad (\alpha=1, 2) \quad (10)$$

where γ is the fluid exchange factor which is governed by the permeability, shape, and porosity of each medium.

The continuity of fluid mass within a unit volume of lumpy clay fillings can be written as

$$\frac{\partial q_{i(\alpha)}}{\partial x_i}+q_{(\alpha)}=-\frac{\partial \varepsilon_{v(\alpha)}}{\partial t} \quad (11)$$

Equation (11) states that the volume change of an element in the lumpy clay domain is due to the flow stored and the exchange of fluid between matrix and inter-lump voids in the element. Equation (11) is rewritten as

$$\begin{cases}\dfrac{\partial \varepsilon_{v(1)}}{\partial t}=-\dfrac{\partial q_{i(1)}}{\partial x_i}+\gamma(p_{(1)}-p_{(2)})\\[2ex] \dfrac{\partial \varepsilon_{v(2)}}{\partial t}=-\dfrac{\partial q_{i(2)}}{\partial x_i}-\gamma(p_{(1)}-p_{(2)})\end{cases} \quad (12)$$

In the paper, the lumpy clay fillings are assumed to be layered homogenously. The distribution of permeability along depth is step-wise and homogenous within a layer. Therefore, from Eqs. (5) ~ (8) and Eq. (12), the continuity equation for lumpy clay fillings is obtained as

$$\begin{cases}\dfrac{k_{ij(1)}}{\gamma_w}\dfrac{\partial^2(p_{(1)})}{\partial x_i \partial x_j}=-\delta_{(1)}\dfrac{\partial^2 u_i}{\partial x_i \partial t}+m_c(\delta_{(2)}-n_{(2)})\dfrac{\partial p_{(1)}}{\partial t}-m_c(\delta_{(2)}-n_{(2)})\dfrac{\partial p_{(2)}}{\partial t}+\gamma(p_{(1)}-p_{(2)})\\[2ex] \dfrac{k_{ij(2)}}{\gamma_w}\dfrac{\partial^2(p_{(2)})}{\partial x_i \partial x_j}=-\delta_{(2)}\dfrac{\partial^2 u_i}{\partial x_i \partial t}-m_c(\delta_{(2)}-n_{(2)})\dfrac{\partial p_{(1)}}{\partial t}+m_c(\delta_{(2)}-n_{(2)})\dfrac{\partial p_{(2)}}{\partial t}-\gamma(p_{(1)}-p_{(2)})\end{cases} \quad (13)$$

Boundary and Initial Conditions

The domain of lumpy clay fillings is denoted as Ω and its boundary is as Γ. The fluids in clay matrix and inter-lump voids are assumed to be full in the domain Ω, which is representated in Fig. 3. The boundary and initial conditions are stated as

(1) Displacement boundary condition:

$$u_i(x, t)=\bar{u}_i(x; t) \quad \forall x\in\Gamma_u,\ t\in T \quad (14a)$$

(2) Traction boundary condition:

$$\sigma_{ij}\hat{n}_j=\bar{T}_i \quad \forall x\in\Gamma_\sigma,\ t\in T \quad (14b)$$

(3) Pore water pressure boundary conditions:

$$\begin{cases}p_{(1)}(x, t)=\bar{p}_{(1)}(x; t) \quad \forall x\in\Gamma_{p(1)},\ t\in T\\ p_{(2)}(x, t)=\bar{p}_{(2)}(x; t) \quad \forall x\in\Gamma_{p(2)},\ t\in T\end{cases} \quad (14c)$$

(4) Flux boundary conditions:

$$\begin{cases}\dfrac{k_{ij}}{\gamma_w}\dfrac{\partial p_{(1)}}{\partial x_j}=-\bar{q}_{i(1)} \quad \forall x\in\Gamma_{q(1)},\ t\in T\\[2ex] \dfrac{k_{ij}}{\gamma_w}\dfrac{\partial p_{(2)}}{\partial x_j}=-\bar{q}_{i(2)} \quad \forall x\in\Gamma_{q(2)},\ t\in T\end{cases} \quad (14d)$$

(5) Initial conditions:

$$\begin{cases}u_i(x; 0)=\bar{u}_{0i}(x)\\ p_{(1)}(x; 0)=\bar{p}_{0(1)}(x) \quad \forall x\in\Omega\\ p_{(2)}(x; 0)=\bar{p}_{0(2)}(x)\end{cases} \quad (14e)$$

where $\hat{n}$ is the outward normal unit vector to the boundary Γ; $\bar{u}_{0i}$, $\bar{p}_{0(1)}$ and $\bar{p}_{0(2)}$ are the initial values; and $\bar{u}_i$, $\bar{T}_i$, $\bar{p}_{(\alpha)}$ and $\bar{q}_{i(\alpha)}$ ($\alpha=1, 2$) are respectively displacement, traction, fluid pressure and fluid flows that are prescribed respectively at Γ_u, Γ_σ, $\Gamma_{p(1)}$, $\Gamma_{p(2)}$, $\Gamma_{q(1)}$ and $\Gamma_{q(2)}$ of Γ, which satisfy

$$\Gamma_u\cup\Gamma_\sigma=\Gamma_{p(1)}\cup\Gamma_{q(1)}=\Gamma_{p(2)}\cup\Gamma_{q(2)}=\Gamma$$
$$\Gamma_u\cap\Gamma_\sigma=\Gamma_{p(1)}\cap\Gamma_{q(1)}=\Gamma_{p(2)}\cap\Gamma_{q(2)}=\varnothing.$$

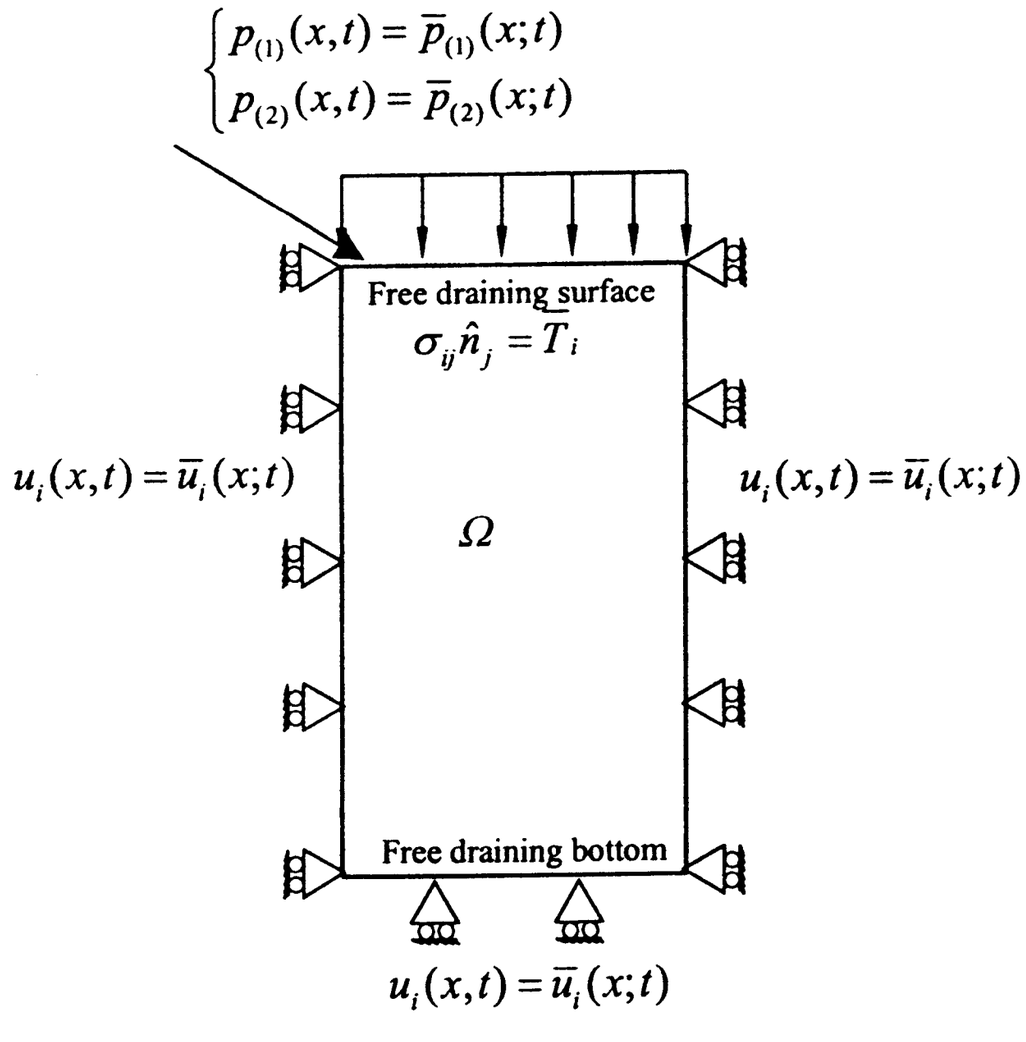

Fig. 3. Boundary conditions for lumpy clay fillings based on double porosity model

NUMERICAL APPROACH

Variational Formulations

Using the variational displacement δu_i as a weight and taking Eq. (7a) and (7b) into consideration, a weak form of the equilibrium equation is written as

$$\int_\Omega \{\delta\varepsilon_{ij}\}^T\{\sigma_{ij}\}d\Omega+\delta_{(1)}\int_\Omega \{\delta u_{i,i}\}^T\{p_{(1)}\}d\Omega + \delta_{(2)}\int_\Omega \{\delta u_{i,i}\}^T\{p_{(2)}\}d\Omega = \int_{\Gamma_\sigma} \{\delta u_i\}^T\{\bar{T}_i\}d\Gamma+\int_{\Gamma_\sigma} \{\delta u_i\}^T\{n_i\}\{p_{(1)}\}d\Gamma + \int_{\Gamma_\sigma} \{\delta u_i\}^T\{n_i\}\{p_{(2)}\}d\Gamma-\int_\Omega \{\delta u_i\}^T\{b_i\}d\Omega \quad (15)$$

Similarly with the variational fluid pressures $\delta p_{(1)}$ and $\delta p_{(2)}$, weak forms of the continuity equations (Eq. 13) are written as

$$\delta_{(1)}\int_\Omega \{\delta p_{(1)}\}^T\{\dot{u}_{i,i}\}d\Omega-\frac{1}{\gamma_w}\int_\Omega \{\delta p_{(1),i}\}[k_{ij(1)}]\{p_{(1),j}\}d\Omega - m_c(\delta_{(2)}-n_{(2)})\int_\Omega \{\delta p_{(1)}\}^T\{\dot{p}_{(1)}\}d\Omega + m_c(\delta_{(2)}-n_{(2)})\int_\Omega \{\delta p_{(1)}\}^T\{\dot{p}_{(2)}\}d\Omega - \gamma\int_\Omega \{\delta p_{(1)}\}^T\{p_{(1)}\}d\Omega+\gamma\int_\Omega \{\delta p_{(1)}\}^T\{p_{(2)}\}d\Omega + \int_{\Gamma_{q(1)}} \{\delta p_{(1)}\}^T\{q_{(1)}\}d\Gamma=0 \quad (16a)$$

$$\delta_{(2)}\int_\Omega \{\delta p_{(2)}\}^T\{\dot{u}_{i,i}\}d\Omega-\frac{1}{\gamma_w}\int_\Omega \{\delta p_{(2),i}\}[k_{ij(2)}]\{p_{(2),j}\}d\Omega + m_c(\delta_{(2)}-n_{(2)})\int_\Omega \{\delta p_{(2)}\}^T\{\dot{p}_{(1)}\}d\Omega - m_c(\delta_{(2)}-n_{(2)})\int_\Omega \{\delta p_{(2)}\}^T\{\dot{p}_{(2)}\}d\Omega + \gamma\int_\Omega \{\delta p_{(2)}\}^T\{p_{(1)}\}d\Omega-\gamma\int_\Omega \{\delta p_{(2)}\}^T\{p_{(2)}\}d\Omega + \int_{\Gamma_{q(2)}} \{\delta p_{(2)}\}^T\{q_{(2)}\}d\Gamma=0 \quad (16b)$$

Spatial Discretization

The meshless method based on the radial Interpolation Method (PIM) (Wang and Liu, 2002) is adopted to discretize the displacement and pore water pressure. The meshless method uses the influence domains instead of elements for interpolation as illustrated in Fig. 4. This largely overcomes the problems associated with the use of elements and facilitates the application of the meshless method to irregular node distributions.

In the process, the interpolation functions are formulated for both displacement and pore water pressure. Stress is the derivative of displacement by the space coordinates. This leads to one-order higher derivatives of the displacement than the pore water pressure in the

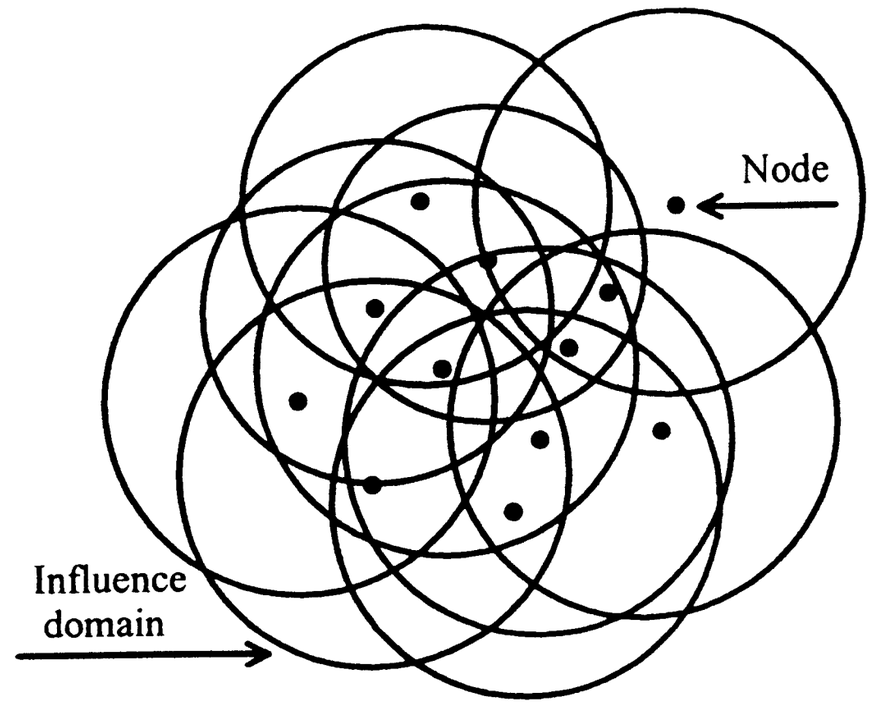

Fig. 4. Influence domain in meshless method

continuity equation. Therefore, the interpolation function for displacement should be one-order higher than that for pore water pressure, for consistent accuracy between the stress and pore water pressure. This unequal order approximation is generally used in finite element method. However, the previously developed radial PIM does not consider it. In order to improve the possible numerical problems caused by inconsistency of accuracy between the displacement and pore water pressures, a one order higher interpolation function is specially used for the displacement than that for the pore water herein (Appendix B). This is the first time that unequal order approximation has been adopted in the meshless methods. Compared to previously developed radial PIM, the unequal order approximation of radial PIM gives higher numerical accuracy.

Using such interpolation functions as shape functions, the displacement and pore water pressure are written as, respectively

$$\boldsymbol{u}(\boldsymbol{x})=\boldsymbol{\Phi}_u(\boldsymbol{x})\boldsymbol{u}^e$$
$$\boldsymbol{p}_\alpha(\boldsymbol{x})=\boldsymbol{\Phi}_p(\boldsymbol{x})\boldsymbol{p}^e_\alpha \quad (17)$$

where $\alpha=1$ and 2 stand respectively for the pore pressures in matrix and inter-lump voids; and $\boldsymbol{\Phi}_u(\boldsymbol{x})$ and $\boldsymbol{\Phi}_p(\boldsymbol{x})$ denote respectively shape functions for displacement and pore water pressures, as explained in the Appendix; and $\boldsymbol{u}^e$ and $\boldsymbol{p}^e$ are the nodal values.

With the relationship in Eq. (17), Eq. (15) and Eqs. (16a) and (16b) written in weak forms are spatially discretized as

$$[\boldsymbol{K}_{11}]\{\boldsymbol{u}\}+\delta_{(1)}[\boldsymbol{K}_{12}]\{\boldsymbol{p}_{(1)}\}+\delta_{(1)}[\boldsymbol{K}_{12}]\{\boldsymbol{p}_{(2)}\}=\{\boldsymbol{R}\} \quad (18a)$$

$$\delta_{(1)}[\boldsymbol{K}_{21}]\{\dot{\boldsymbol{u}}\}-[[\boldsymbol{K}_{22}]+\gamma[\boldsymbol{K}_{23}]]\{\boldsymbol{p}_{(1)}\}+\gamma[\boldsymbol{K}_{23}]\{\boldsymbol{p}_{(2)}\} - a[\boldsymbol{K}_{23}][\{\dot{\boldsymbol{p}}_{(1)}\}-\{\dot{\boldsymbol{p}}_{(2)}\}]=\{\boldsymbol{Q}_{(1)}\} \quad (18b)$$

$$\delta_{(2)}[\boldsymbol{K}_{21}]\{\dot{\boldsymbol{u}}\}-[[\boldsymbol{K}_{24}]+\gamma[\boldsymbol{K}_{23}]]\{\boldsymbol{p}_{(2)}\}+\gamma[\boldsymbol{K}_{23}]\{\boldsymbol{p}_{(1)}\} + a[\boldsymbol{K}_{23}][\{\dot{\boldsymbol{p}}_{(1)}\}-\{\dot{\boldsymbol{p}}_{(2)}\}]=\{\boldsymbol{Q}_{(2)}\} \quad (18c)$$

where, with the assumption of zero pore water pressures on traction boundary,

$$[K_{11}]=\int_{\Omega} B_1^T D B_1 d\Omega \quad [K_{12}]=\int_{\Omega} B_2 \Phi_p d\Omega$$

$$[R]=\int_{\Gamma_\sigma} \Phi_u^T T d\Gamma+\int_{\Omega} \Phi_u^T b d\Omega \quad [K_{21}]=\int_{\Omega} (B_2\Phi_p)^T d\Omega$$

$$[K_{22}]=\frac{1}{\gamma_w}\int_{\Omega} B_3^T K_{(1)} B_3 d\Omega \quad [K_{23}]=\int_{\Omega} \Phi_p^T \Phi_p d\Omega$$

$$[K_{24}]=\frac{1}{\gamma_w}\int_{\Omega} B_3^T K_{(2)} B_3 d\Omega$$

$$\{Q_{(1)}\}=-\int_{\Gamma_{q(1)}} \{\Phi_p\}^T q_{(1)} d\Gamma \quad \{Q_{(2)}\}=-\int_{\Gamma_{q(2)}} \{\Phi_p\}^T q_{(2)} d\Gamma$$

$$B_1=\begin{bmatrix} \dfrac{\partial \Phi_u}{\partial x_1} & 0 \\ 0 & \dfrac{\partial \Phi_u}{\partial x_2} \\ \dfrac{\partial \Phi_u}{\partial x_2} & \dfrac{\partial \Phi_u}{\partial x_1} \end{bmatrix} \quad B_2=\begin{bmatrix} \dfrac{\partial \Phi_u}{\partial x_1} \\ \dfrac{\partial \Phi_u}{\partial x_2} \end{bmatrix} \quad B_3=\begin{bmatrix} \dfrac{\partial \Phi_p}{\partial x_1} \\ \dfrac{\partial \Phi_p}{\partial x_2} \end{bmatrix}$$

$$a=m_c(\delta_{(2)}-n_{(2)})$$

It is understood in the above expressions that: $K_{(1)}$ is the permeability matrix of clay matrix; $K_{(2)}$ is the permeability matrix of the inter-lump porous medium; T is the surface traction matrix; D is the material matrix of linear elasticity; and $q_{(1)}$ and $q_{(2)}$ are the matrices of boundary flux.

Temporal Discretization

The time domain is discretized through the finite difference method. In this manner, a function $f(x)$ integrated from t to $t+\Delta t$ is expressed as

$$\int_t^{t+\Delta t} f(x)dx=\Delta t[\theta f(t)+(1-\theta)f(t+\Delta t)] \tag{19}$$

where t and Δt denote time and time increment, respectively; and $\theta=0$, 0.5 and 1 correspond respectively to the fully explicit Euler algorithm, Crank-Nicolson algorithm and backward Euler algorithm. After time discretization by using Eq. (19), Eqs. (18a)~(18c) are rewritten as, respectively

$$[K_{11}]\{\Delta u\}^{t+\Delta t}+\delta_{(1)}[K_{12}]\{\Delta p_{(1)}\}^{t+\Delta t}+\delta_{(1)}[K_{12}]\{\Delta p_{(2)}\}^{t+\Delta t}=[\Delta R] \tag{20a}$$

$$\delta_{(1)}[K_{21}]\{\Delta u\}-[\theta\Delta t[K_{22}]+(a+\gamma\theta\Delta t)[K_{23}]]\{\Delta p_{(1)}\}+(a+\gamma\theta\Delta t[K_{23}])\{\Delta p_{(2)}\}=\Delta t[[K_{22}]+\gamma[K_{23}]]p^t_{(1)}-\Delta t\gamma[K_{23}]p^t_{(2)}+[\Delta Q_{(1)}] \tag{20b}$$

$$\delta_{(2)}[K_{21}]\{\Delta u\}+(a+\gamma\theta\Delta t[K_{23}])\{\Delta p_{(1)}\}-[\theta\Delta t[K_{24}]+(a+\gamma\theta\Delta t[K_{23}]])\{\Delta p_{(2)}\}=-\Delta t\gamma[K_{23}]p^t_{(1)}+\Delta t[[K_{24}]+\gamma[K_{23}]]p^t_{(2)}+[\Delta Q_{(2)}] \tag{20c}$$

VERIFICATIONS

Implementation of the Radial PIM Meshless Method

In the present meshless method based on the radial PIM, the order of the interpolation function for the displacement is one order higher than that for the excess pore water. This is reflected by adopting linear polynomials (m in Appendix A is equal to 3) for the pore water pressures and quadric polynomials (m in Appendix A is equal to 6) for the displacement. The minimum radius of each influence domain is generally taken as 1.5 m. Radial PIM meshless method requires certain number of nodes to construct the shape function. It is found that around 6 to 30 numbers of nodes can lead to good results in the preliminary numerical studies; otherwise reasonable results can not be obtained. Hence, if the number of nodes contained in an influence domain is less than 6, its radius of the domain is enlarged to encompass at least 6 nodes. The shape parameter for a Gaussian type function (b in Eq. (38) in Appendix A) is 2.01. It is found that, when orders of interpolation functions are mutually unequal between those for pore water pressure and displacement, the backward Euler algorithm ($\theta=1$) in time integration can avoid spurious oscillation in the radial PIM meshless method [Wang et al. 23]. Hence, the backward Euler algorithm is used for computation herein.

A suitable pattern of nodal arrangement is examined. For a typical one-dimensional problem as shown in Fig. 5(a), nodes are arranged as in Fig. 5(b) for regular distribution and Fig. 5(c) for irregular distribution. The top surface is fully permeable for the clay matrix and the inter-lump structure and bottom surface is rigid and impervious. The soil layer is 10 m thick. A uniform load of 10 kPa is applied to the top surface. Material constants used in the computation are $E=10$ MPa, $\nu=0$, $k_{(1)}=1\times10^{-4}$ m/year, $k_{(2)}=1\times10^{-1}$ m/year, $n_{(2)}=0.1$, and $\gamma=1\times10^{-4}$. Figure 6 shows the effect of node distribution on the history of pore water pressure dissipation at the base of the lumpy clay fillings. The results obtained with irregular node distribution almost match those obtained with regular node distribution for both the matrix and in inter-lump voids. Hence, it can be confirmed that the current numerical approach is not sensitive to the way of node distribution. In the following computation, only regular node distribution is used.

Comparison with Other Numerical Methods

One-dimensional consolidation of fissured clay has been previously formulated and analyzed with the double porosity model by using the finite element method (Khalili et al., 1999) and the matrix transfer method (Li, 2002). Since the computational approach developed in this paper is also applicable to fissured clay, these analyzed cases are also analyzed by this method for verification of the formulation and computer code first. In this study, the time factor T_v is defined as

$$T_v=\frac{k_{(1)}+k_{(2)}}{m\gamma_w d^2}t \tag{21}$$

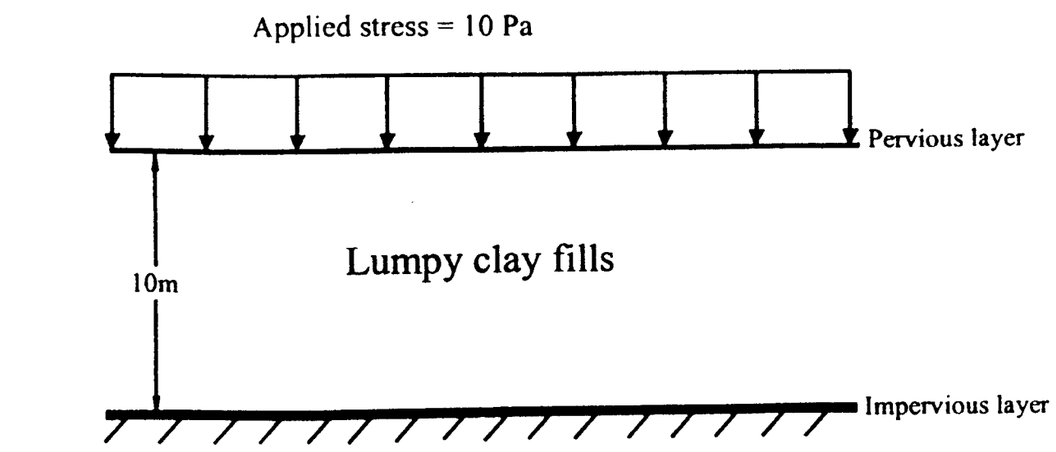

(a) 1D consolidation problem

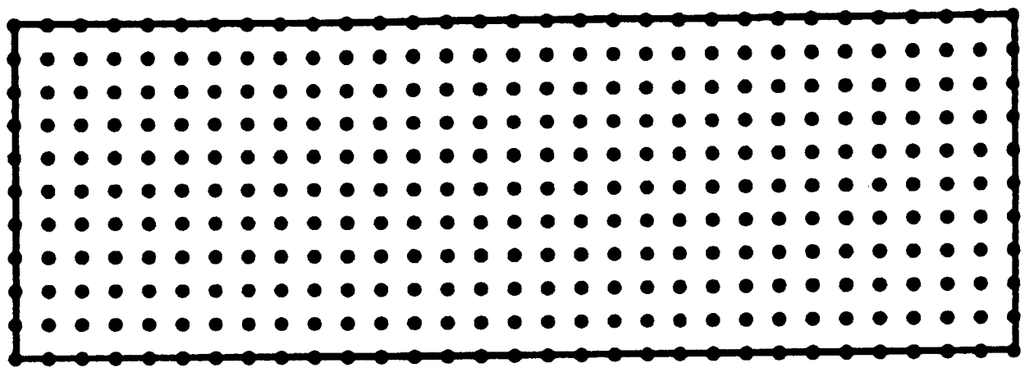

(b) Regular nodal distribution (341 nodes)

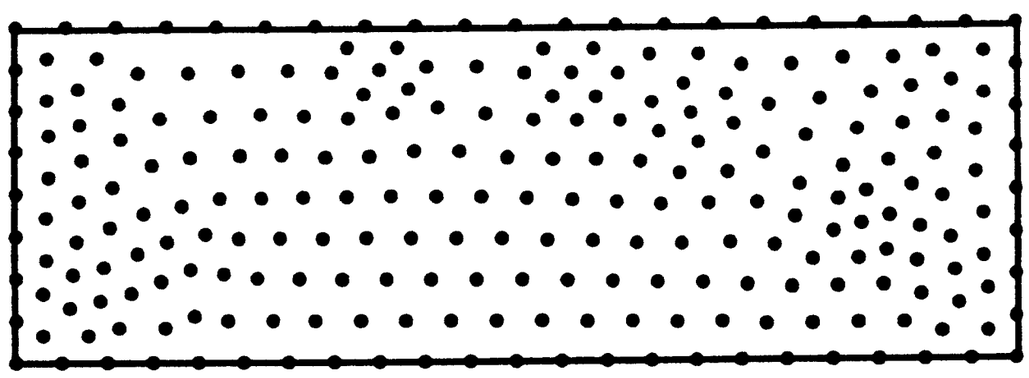

(c) Irregular nodal distribution (248 nodes)

Fig. 5. Conditions and nodal distributions considered

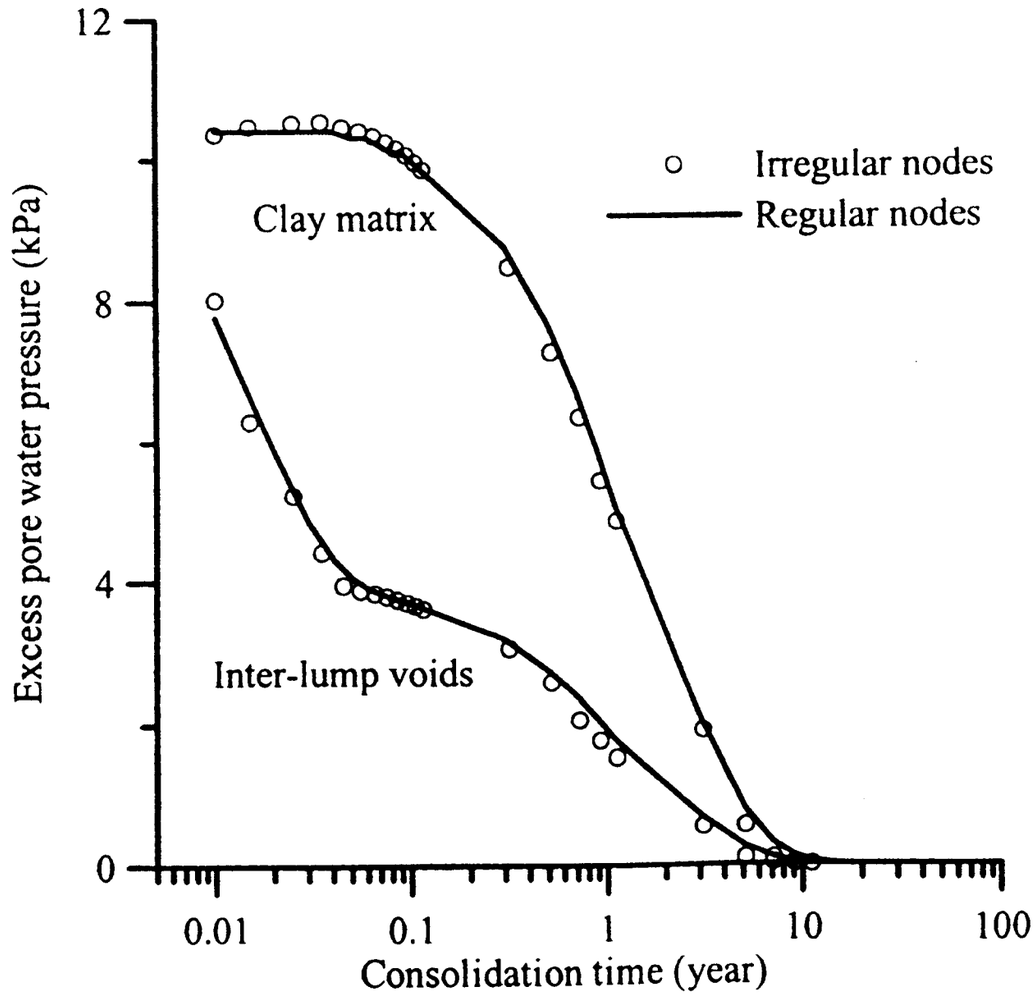

Fig. 6. Effects of difference in node distribution on pore water pressure

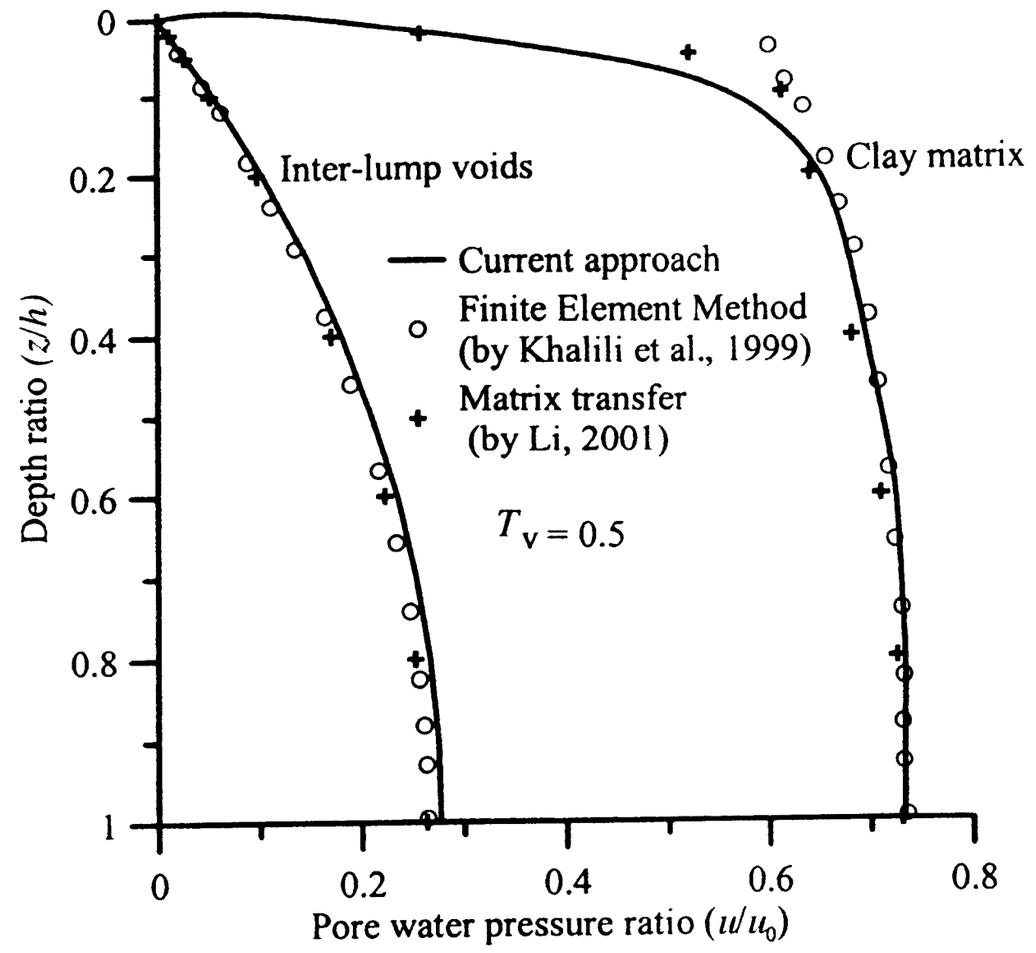

Fig. 7. Pore water pressure distributions with depth computed by various methods

where d is the maximum drainage path and $k_{(1)}$ and $k_{(2)}$ are isotropic. Also, average degrees of consolidation for the clay matrix, inter-lump voids and overall lumpy clay system are defined as, respectively

$$U_{(1)} = 1 - \frac{\int_0^h p_{(1)} dz}{\int_0^h \bar{p}_{(01)} dz} \tag{22a}$$

$$U_{(2)} = 1 - \frac{\int_0^h p_{(2)} dz}{\int_0^h \bar{p}_{(02)} dz} \tag{22b}$$

$$U = \frac{S_t}{S_\infty} \tag{22c}$$

where S_t and S_∞ are respectively the surface settlement at time t and the ultimate surface settlement; $U_{(1)}$, $U_{(2)}$ and U are respectively average degrees of consolidation for the clay matrix, inter-lump voids (fissures) and overall lumpy clay system (overall fissured clay).

Figure 7 shows the distributions of excess pore water pressures along depth in the matrix and inter-lump voids at $T_v = 0.5$. Figure 8 shows the variation of the average degree of consolidation with time for the overall system. Good agreements are observed among the results computed by the three different methods.

Centrifuge Test

The experiments have been conducted at the National University of Singapore Geotechnical Centrifuge to study the consolidation behavior of the lumpy clay fillings. Details of this centrifuge are described in Lee et al. (1991). To study the consolidation and deformation characteristics of lumpy clay fillings physically, Wong

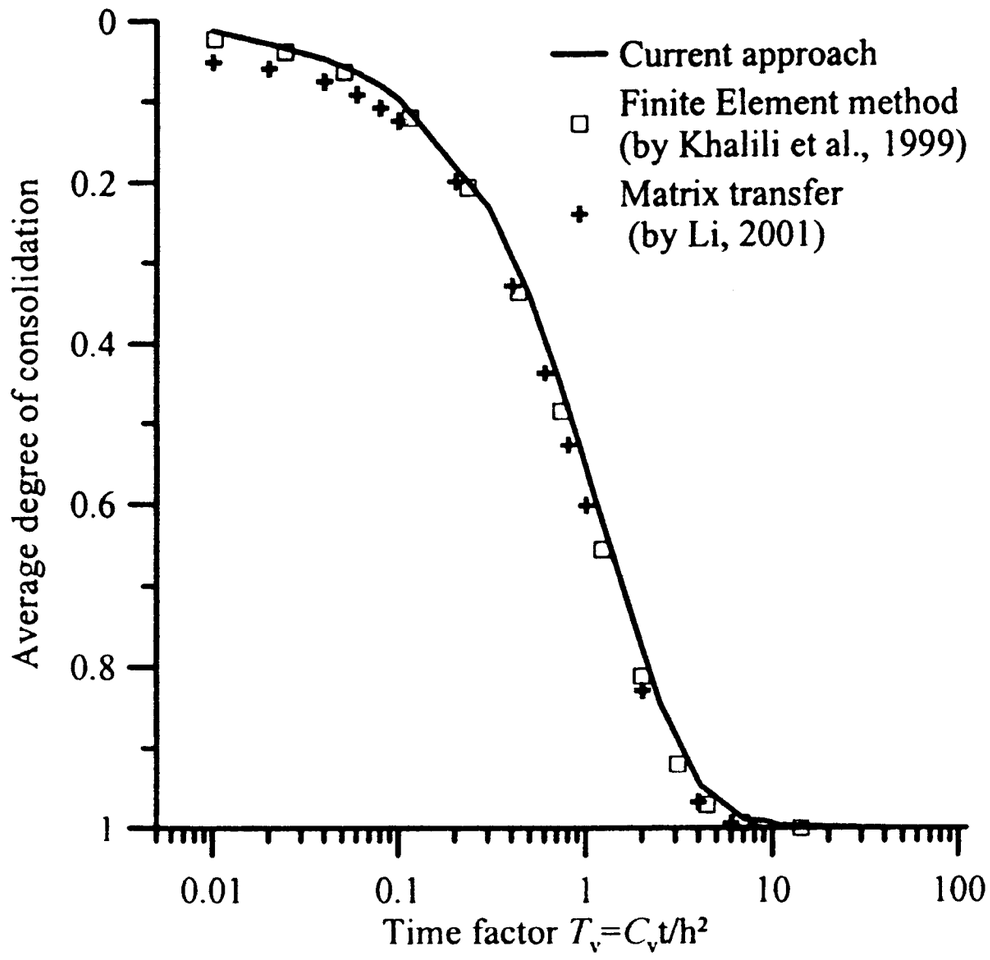

Fig. 8. Average degree of consolidation versus time factor computed by various methods

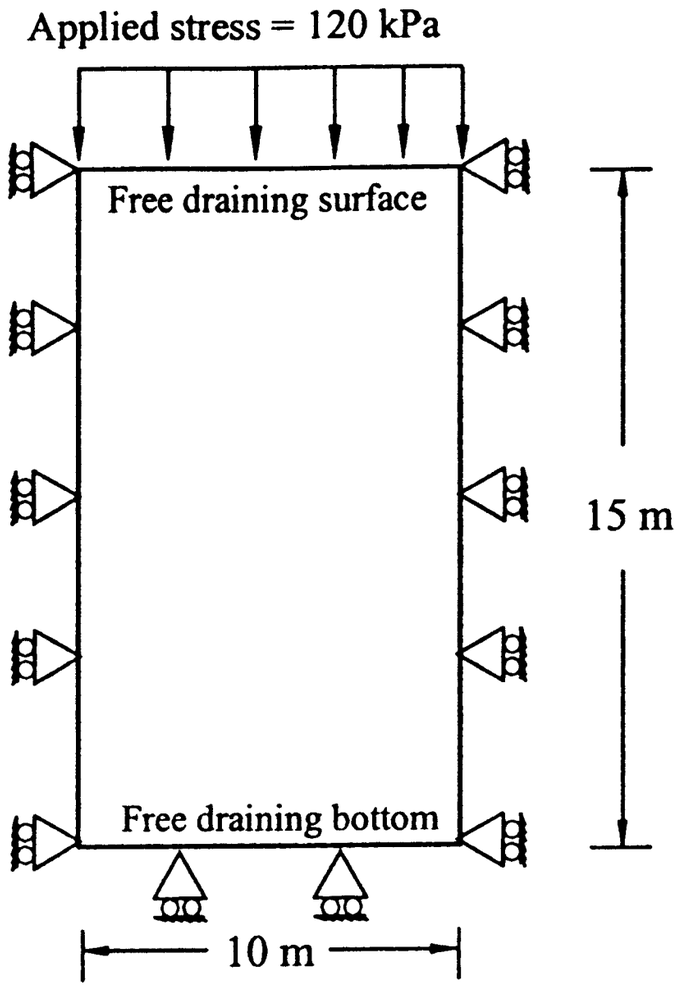

(a) Schematic view of boundary conditions of the soil in centrifuge test (in prototype)

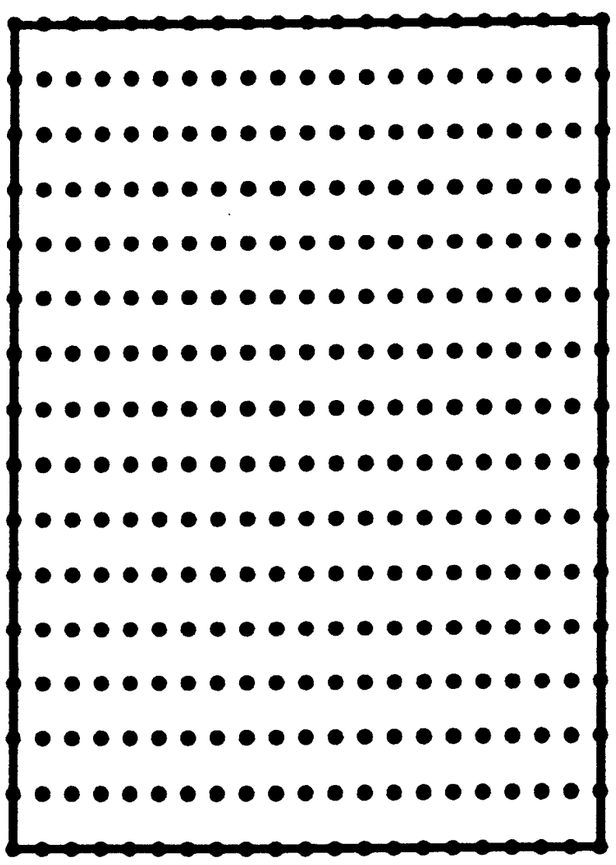

(b) Node distribution used in meshless method analysis (336 nodes)

Fig. 9. Conditions used in test 1 and analysis

Table 1. Parameters in numerical computation for centrifuge model test 1

Parameter	Definition	Magnitude	Unit
m	Overall compressibility of lumpy clay fill	6.2×10^{-3}	kPa^{-1}
m_c	Compressibility of the clay matrix	9.3×10^{-4}	kPa^{-1}
$k_{(1)}$	Permeability of clay matrix	3×10^{-4}	m/year
$k_{(2)}$	Permeability of inter-lumpy voids	3×10^{-1}	m/year
v	Poisson's ratio	0.35	—
E	Drained bulk modulus	870	KPa
$n_{(2)}$	Porosity of inter-lump void	0.2	—
γ	Fluid exchange factor	4.5×10^{-5}	—

Table 2. Different distributions of $k_{(2)}$ and m used in computation for centrifuge test 1

	Case 1	Case 2	Case3
Part A: Distribution of $k_{(2)}$	Surface $1k_{(2)}$ Lumpy clay Bottom $1k_{(2)}$	Surface $1.2k_{(2)}$ Bottom $0.8k_{(2)}$	Surface $1.9k_{(2)}$ Bottom $0.1k_{(2)}$
Part B: Distribution of m	Surface $1m$ Lumpy clay Bottom $1m$	Surface $1.2m$ Bottom $0.8m$	Surface $1.9m$ Bottom $0.1m$

(1997) used uniform size of dredged clay lumps in experiments, while Maninannan (1999) carried out centrifuge tests with different size lumpy clays. Their centrifuge tests were conducted under 100 g. In the tests, the model setup consisted of a strong box with its frontal portion made of perspex that allowed the entire test process to be captured on a video camera. The lumpy clay used in the studies was taken from the New Container Terminal site in Singapore. By using a cylindrical scoop, the clay balls were taken from the recompressed soil in the tub. The clay balls were then placed by hand in hexagonal face packing in layers in the container. Thumb pins were at-

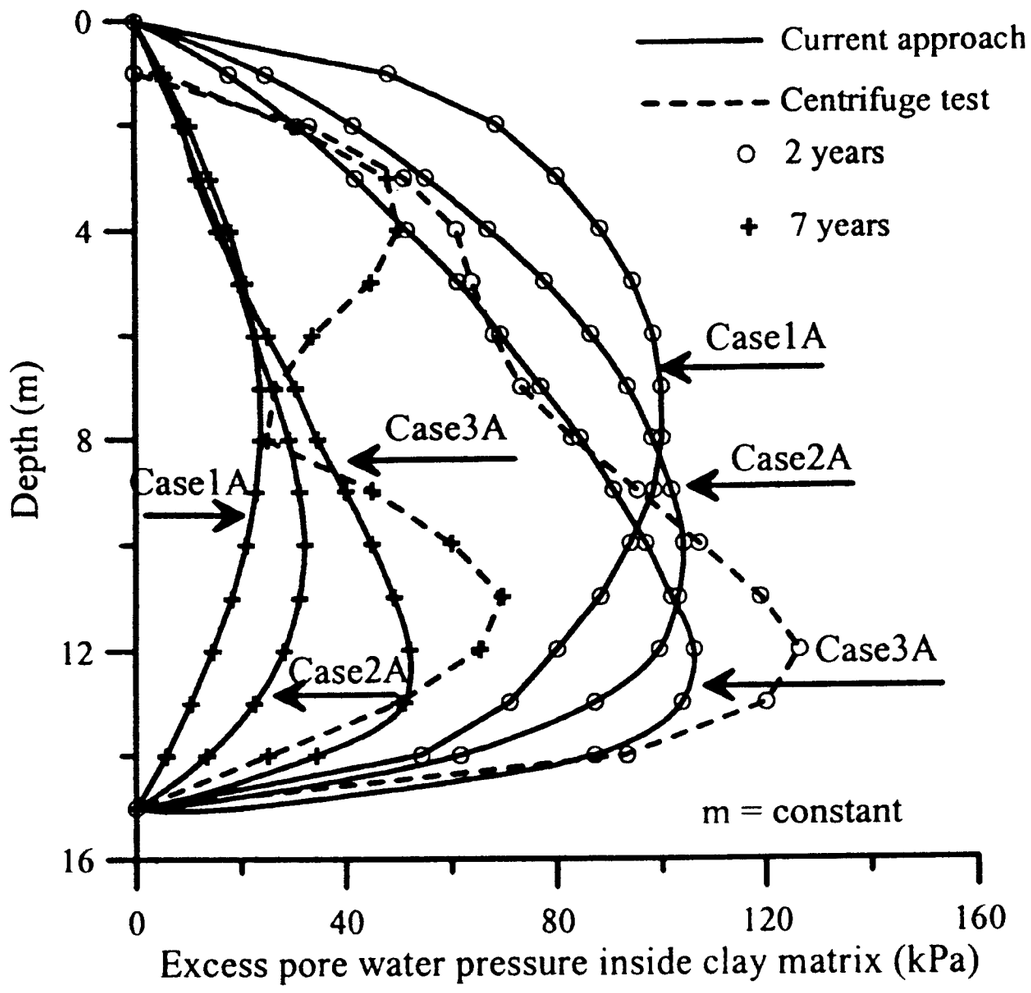

(a) Excess pore water pressure in clay matrix

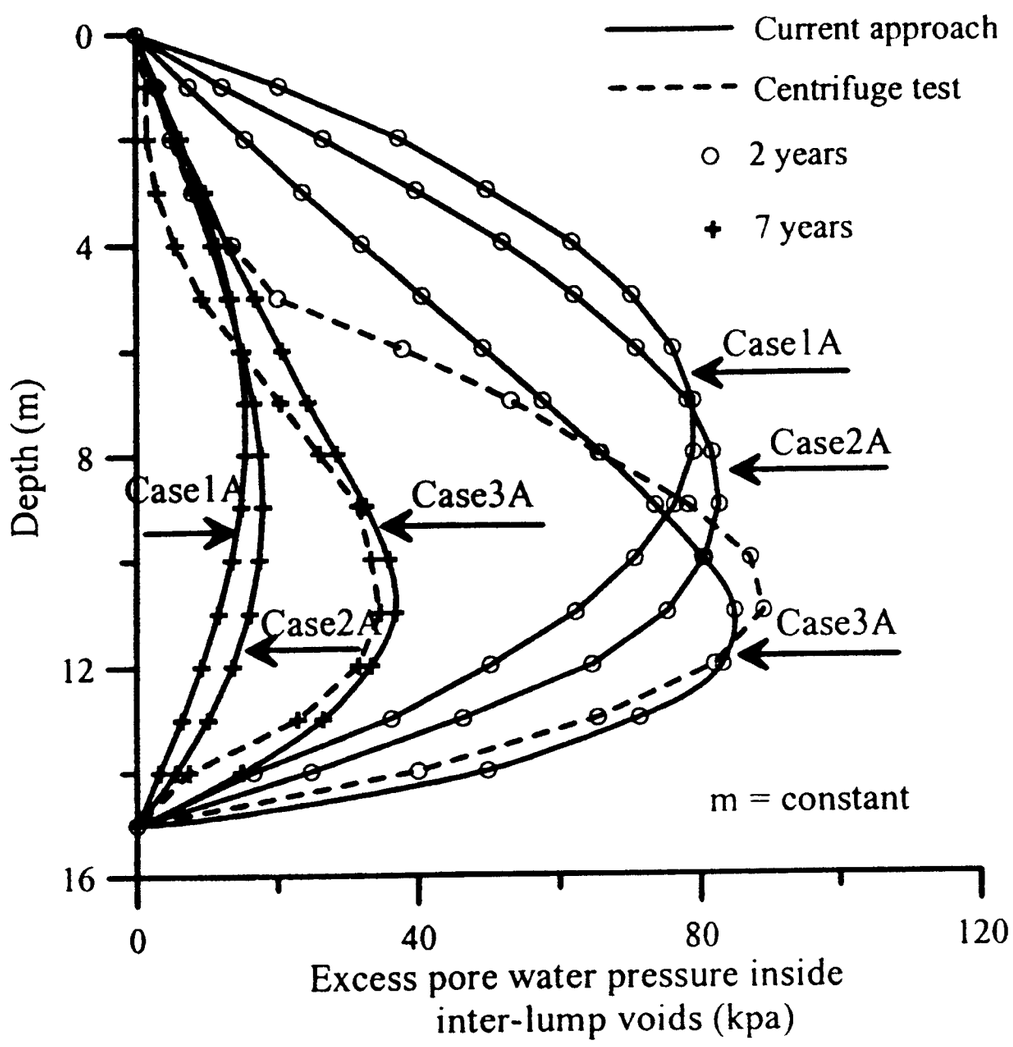

(b) Excess pore water pressure in inter-lump voids

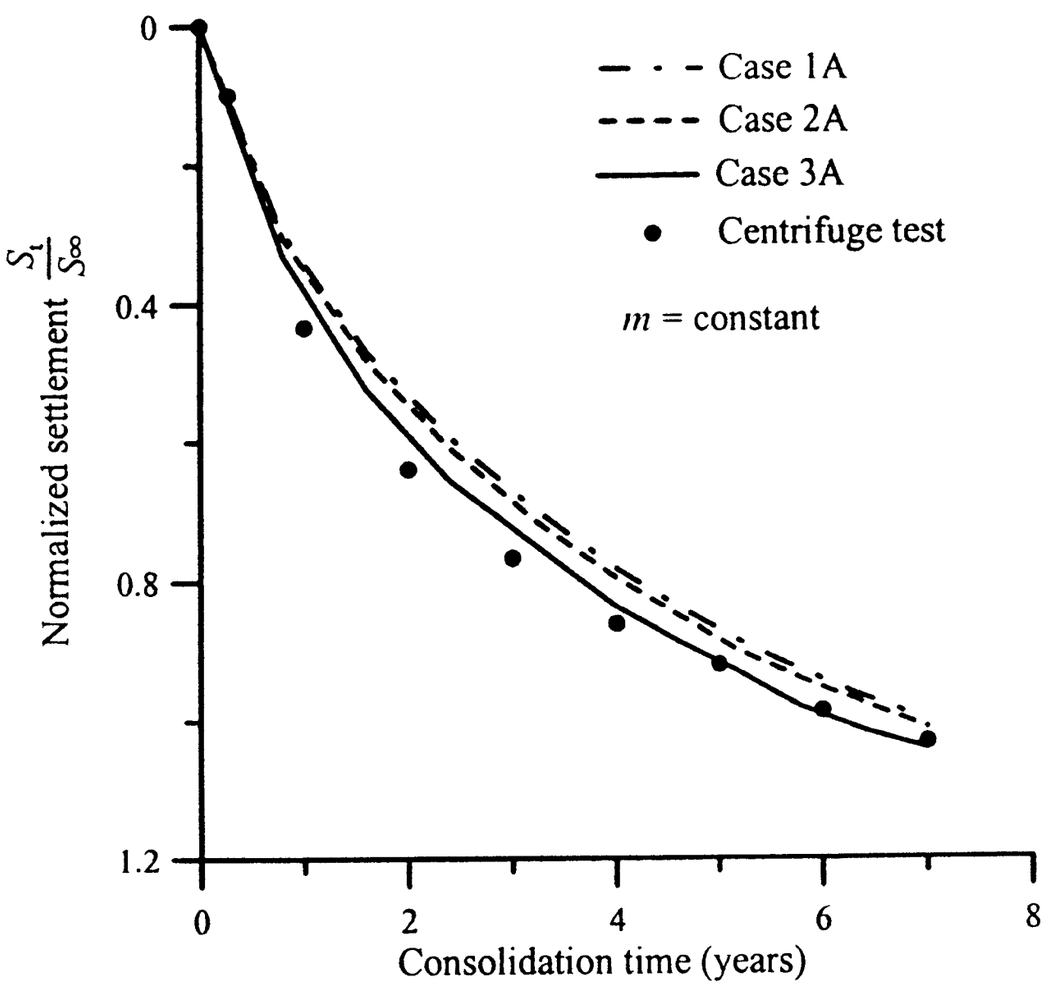

(c) Normalized settlement (S_t: surface settlement; S_∞: final settlement)

Fig. 10. Comparison of test results and numerical results for different distributions of $k_{(2)}$ along depth (test 1)

tached onto the surface of selected clay balls located close to the perspex wall. The pins were made to face outward, such that their movements could be measured with reference to the measuring tapes placed on the cylinder. Further details of the experimental set-up for lumpy clay fillings consolidation are given in Wong (1997). Two centrifuge model tests were conducted to study the consolidation characteristics of lumpy clay fillings in the one-dimensional condition (Leung et al., 1996, 2001; Wong, 1997). They were conducted under the pressures 260 kPa and 120 kPa applied on the surface in each test.

The developed numerical method is examined by using these test results, mainly with respect to the applicability of the double porosity model for the consolidation analysis of lumpy clay fillings.

The basic parameters involved in the governing equations for lumpy clay fillings are λ, G, $n_{(2)}$, m_c, m, $k_{(1)}$, $k_{(2)}$ and γ. The large-scale one-dimensional drained compression tests were also conducted on clay lumps, when the centrifuge model tests were conducted. The average values of m and $n_{(2)}$ over the depth are estimated from the compression tests conducted on clay lumps (Wong, 1997). m_c and n_2 are estimated from element tests conducted on clay matrix (Wong, 1997). Since the consolidation behavior of lumpy clay fillings is governed by $k_{(2)}$ at the early stage of the consolidation process, $k_{(2)}$ is estimated at the early stage observed in the large scale test on clay lumps. On the other hand, $k_{(1)}$ is estimated mainly at a very late stage of consolidation process observed in the above tests. Past experience with similar clay and the finite element analysis are also utilized to estimate the rest of parameters (Mannivanann, 1999) except γ. Modifying the expression originally proposed by Warren and Root (1963) for rock mass with fissure networks, the fluid exchange factor γ for lumpy clay fillings is estimated from

$$\gamma = \frac{\xi k_{(1)}}{l^2 \gamma_w} \tag{23}$$

where ξ is the shape factor of the clay matrix and l is the equivalent average diameter of clay lumps. Table 1 summarizes these estimated values of the parameters. Because detailed material information on lumpy clay fillings during the centrifuge tests is not available, several distributions of the parameters along depth are considered based on the above estimated average values over the depth. They are listed in Table 2. Figure 9 shows the

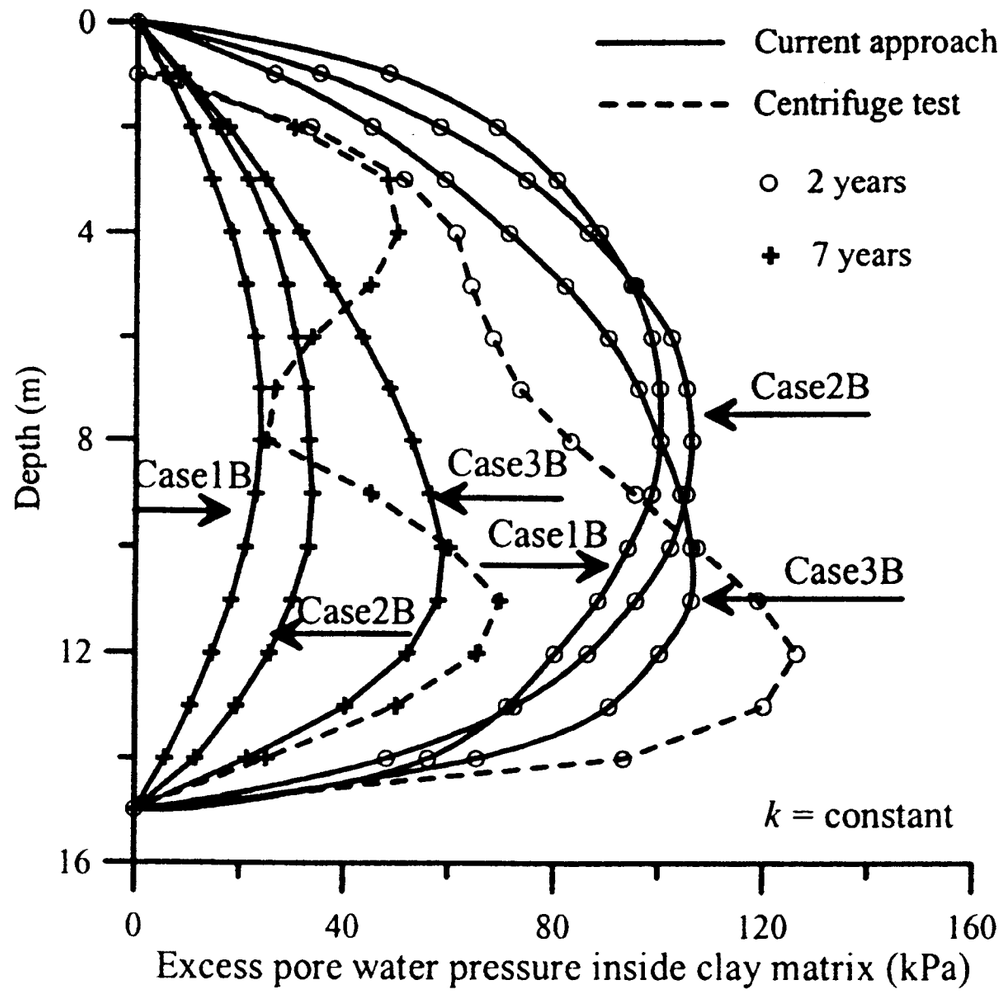

(a) Excess pore water pressure in clay matrix

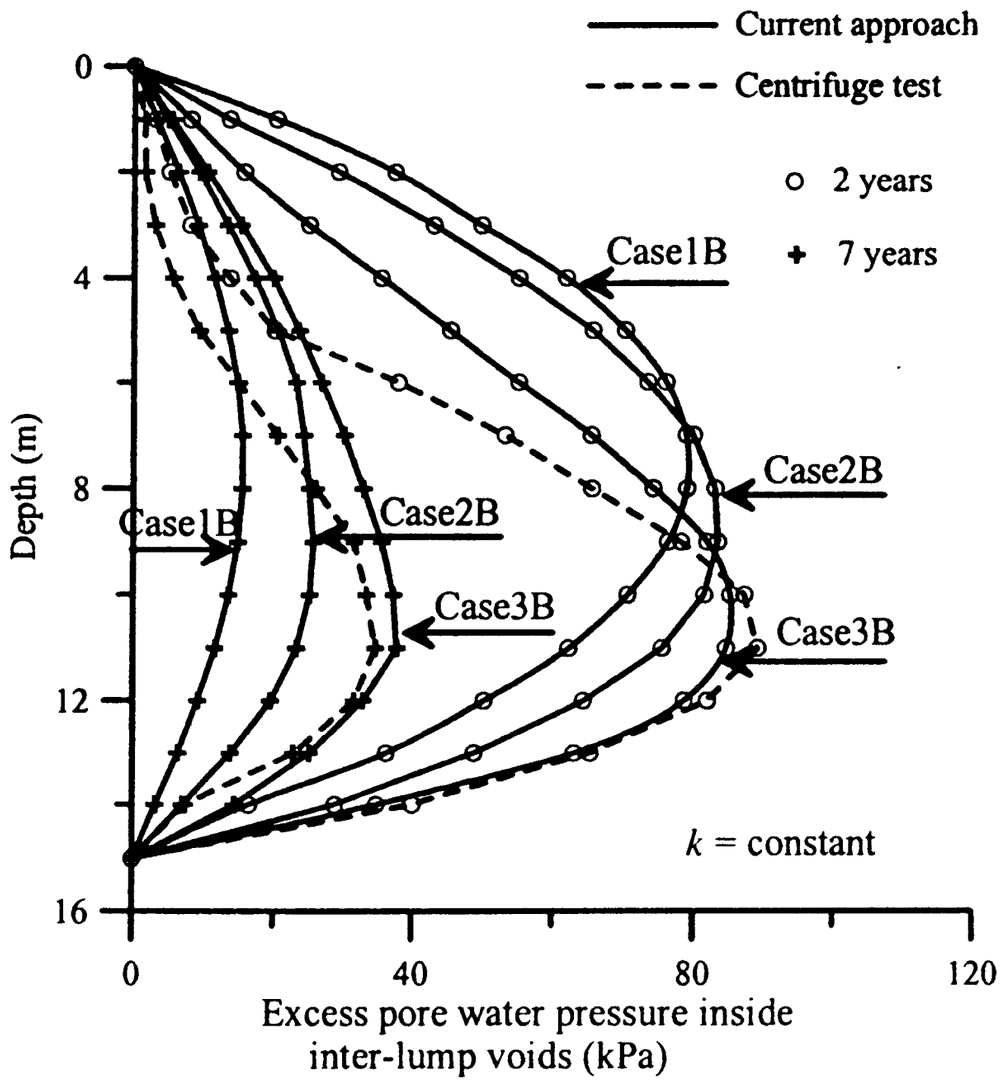

(b) Excess pore water pressure in inter-lump voids

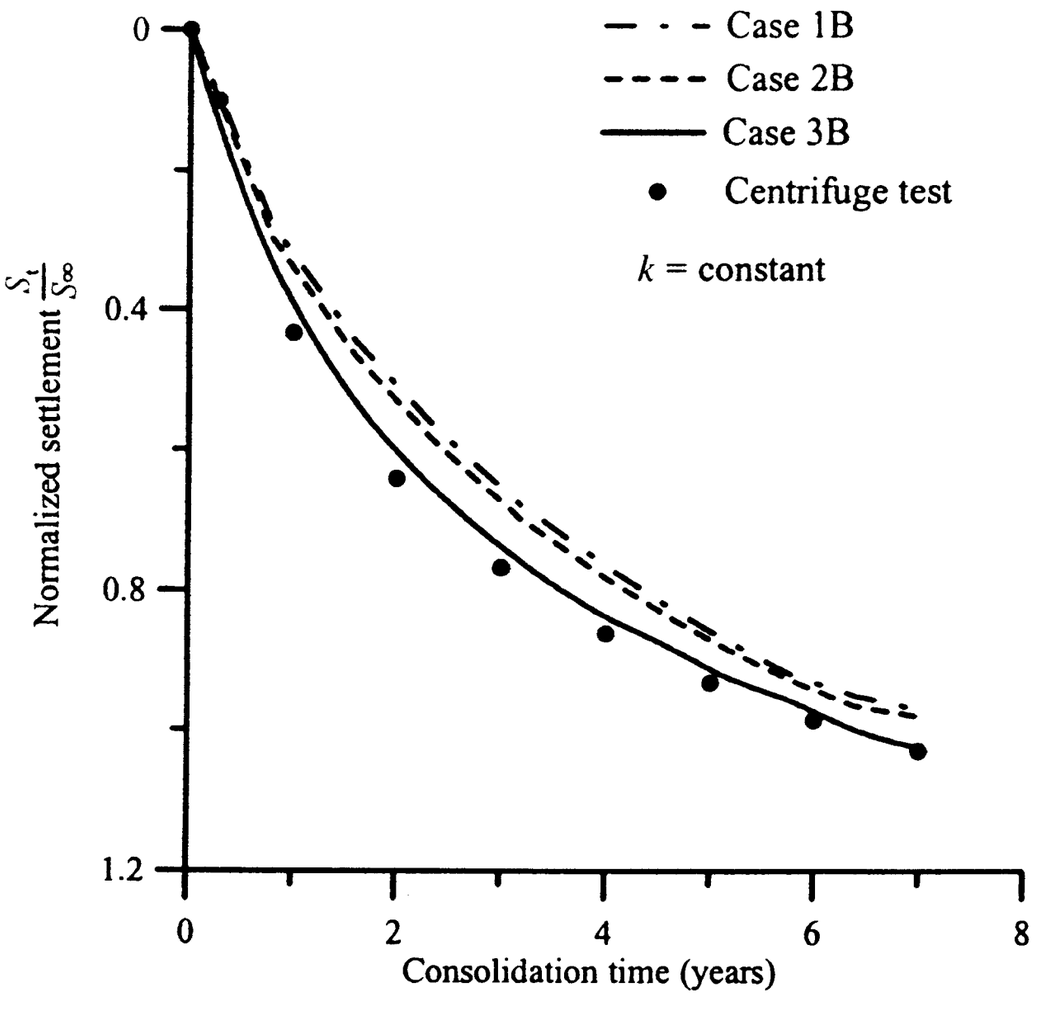

(c) Normalized settlement

Fig. 11. Comparison of test results and numerical results for different distributions of *m* along depth (test 1)

arrangement of nodes and the boundary conditions used for the analyses.

Numerical results computed for the first centrifuge test are shown in Figs. 10 ~ 12 for pore water pressure distributions along the depth at two different times and for time histories of the surface settlement. The results in Fig. 10 are obtained for various distributions of k_2 with depth while keeping m uniform along the depth. The results in Fig. 11 are obtained for various distributions of m with depth while keeping $k_{(2)}$ uniform along the depth.

The results in Fig. 12 are obtained when both $k_{(2)}$ and m vary with depth according to Case 3. It is confirmed in these figures that the used parameters with distributions of $k_{(2)}$ and m according to Case 3 can produce computed results close to those observed in the centrifuge test for both pore water pressures in the matrix and inter-lump voids.

Since the experimental setup and model for lumpy clay in the second test were practically the same as those in the first test except for the intensity of applied pressure, the numerical results are computed with the parameters which were confirmed in the first test results. The second test results are now compared with the numerical results in Fig. 13. Good agreement between the numerical and experimental results are observed for both excess pore water pressures in the matrix and inter-lump voids. Based on Eq. (23) that was originally proposed for the rock mass, the fluid exchange factor, γ, can be estimated somewhere from 4×10^{-5} to 5×10^{-5}. For this reason, the numerical results computed with $\gamma=4\times10^{-5}$ and 5×10^{-5} are also shown in Fig. 13 for comparison. It is seen in the figure that parameter γ in this range alters the numerical results relatively little and those with $\gamma=4\times10^{-5}$ are still in good agreement with the test results. The above comparisons imply that the double porosity model can predict the consolidation behavior of lumpy clay fillings reasonably well. Therefore, the current approach appears to be effective provided that proper material properties are given.

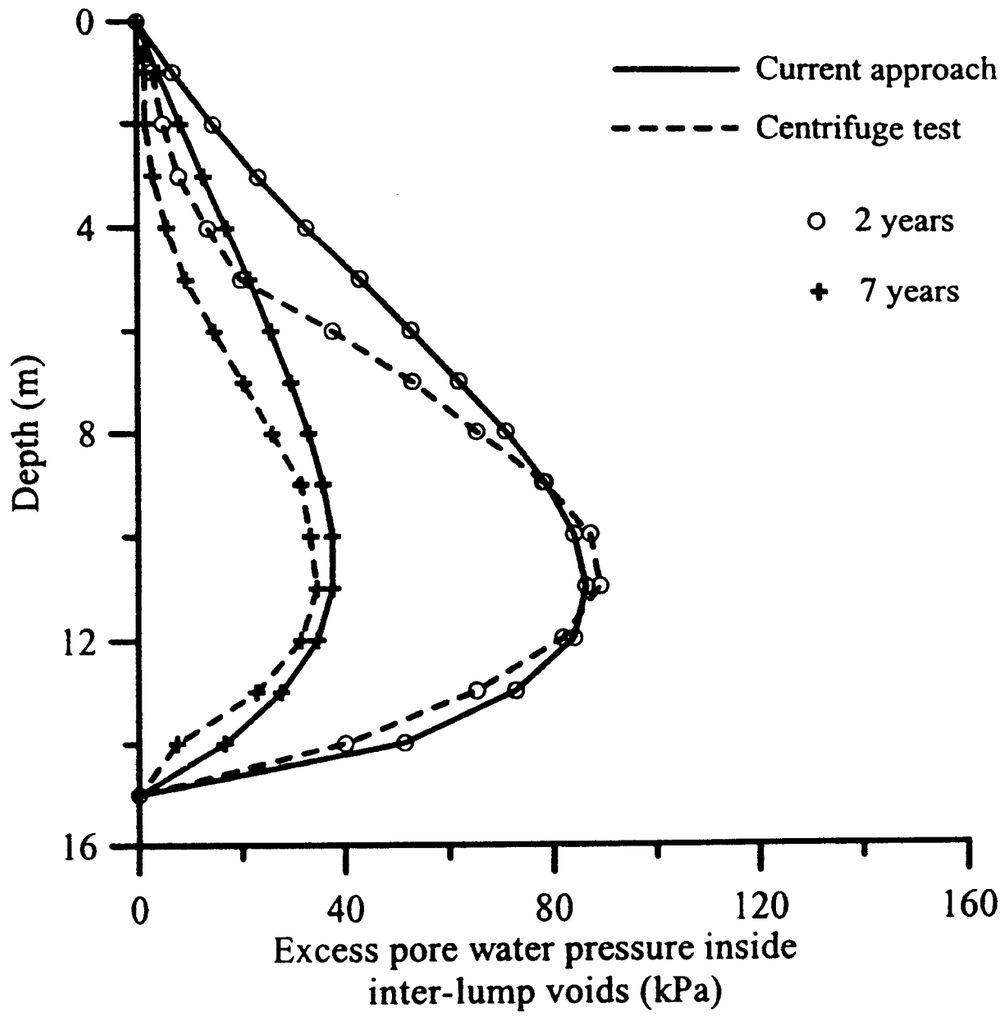

(a) Excess pore water pressure in clay matrix

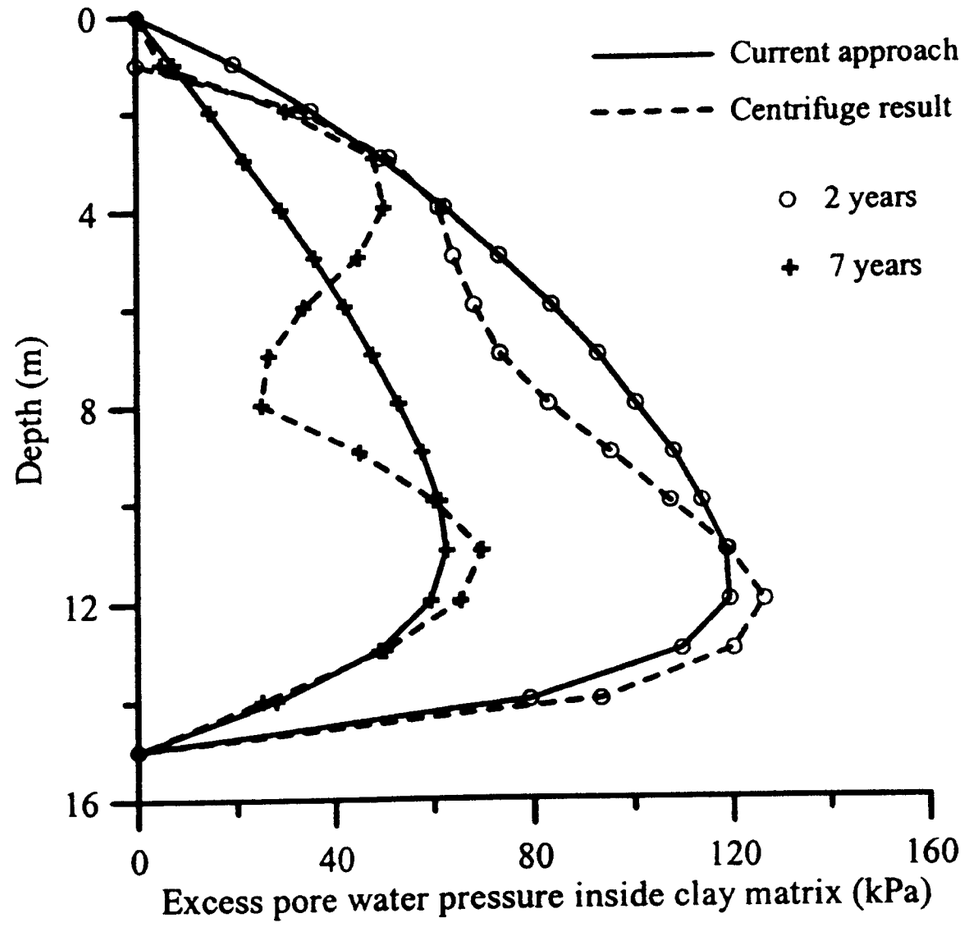

(b) Excess pore water pressure in inter-lump voids

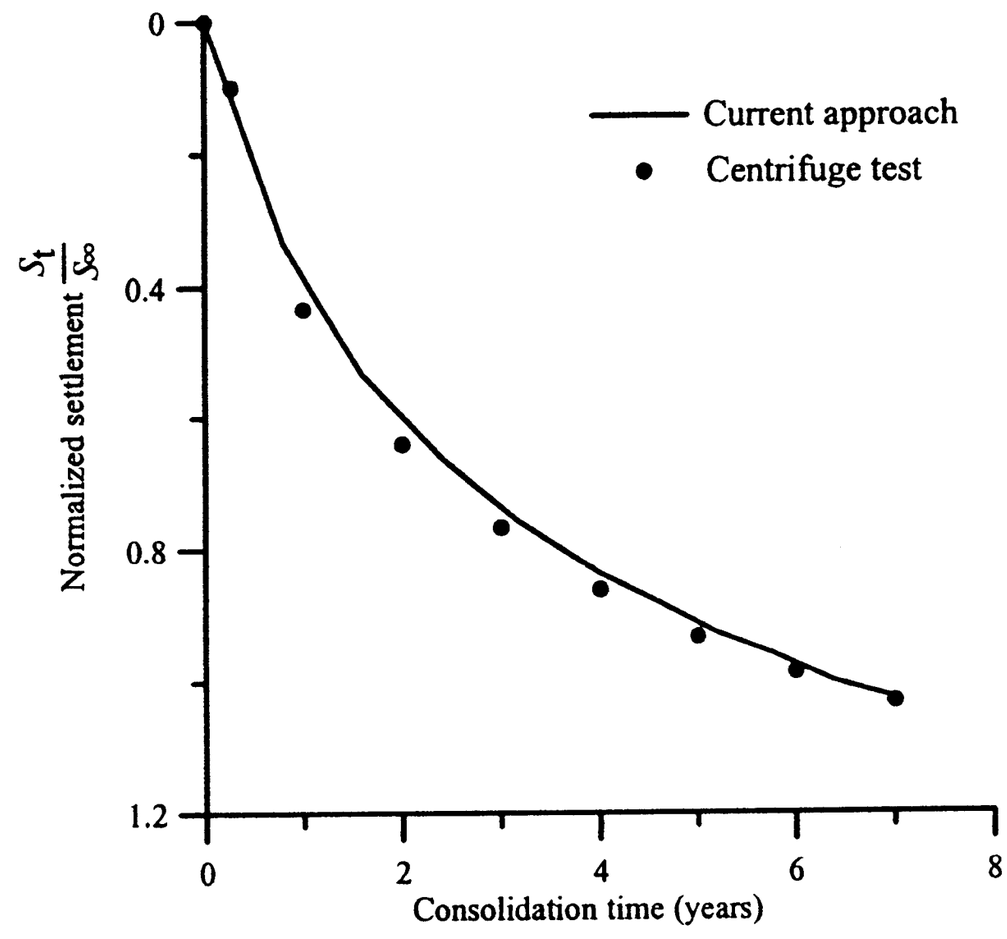

(c) Normalized settlement

Fig. 12. Comparison of test results and numerical results with Case 3 distribution of both m and $k_{(2)}$ along depth (test 1)

CONSOLIDATION BEHAVIOUR OF LUMPY CLAY FILLINGS

In this section numerical experiments are carried out to study the consolidation behavior of lumpy clay fillings for one-dimensional and two-dimensional problems.

One-dimensional Consolidation Problem

Figure 14 shows typical variations of average degrees of consolidation with time in the matrix and inter-lump voids. Three distinct stages are observed in the consolidation behavior of lumpy clay fillings. Stage I is characterized by the rapid dissipation of excess pore water pressure in inter-lump voids but very little dissipation in the matrix. This is due to a higher permeability in inter-lump voids and a lower permeability in the matrix. As a result, the pore water pressure drops quickly in inter-lump voids and more load is transferred from the inter-lump voids to the clay matrix, which leads to a fluid pressure raise in the clay matrix before it starts to dissipate and hence the average degree of consolidation for the clay matrix is slightly larger than 1. Stage II is characterized by a significant exchange of fluid between the matrix and inter-lump voids, in which the pore water in the matrix leaks into inter-lump voids rather significantly due to the pressure difference developed between the matrix and inter-lump voids. The leak from the matrix slowdowns the rate of pore pressure dissipation within inter-lump voids. The duration of this stage depends mainly on the fluid exchange factor (γ). This fluid exchange is governed by the average porosity of inter-lump voids and the permeability of the matrix as expressed by Eq. (23). The larger fluid exchange factor results in a shorter duration of stage II. The last stage or stage III is characterized by a dominant dissipation of pore water pressure in the matrix since most of the pore water in the inter-lump voids has dissipated at stage III.

For the one-dimensional consolidation problem, numerical experiments are conducted to study the effects of variations of the fluid exchange factor, γ, permeability ratio, $R_k(=k_{(2)}/k_{(1)})$, and compressibility ratio, $\delta_1(=m_c/m)$. Figure 15 shows the effect of variation of R_k on the average degree of consolidation, defined as S_t/S_∞. As R_k gets smaller, the permeability of inter-lump voids becomes closer to that of the clay matrix. This situation occurs as the openings of inter-lump voids are reduced in the consolidation process. When it progresses to a significant degree, inter-lump voids become not as effective in draining and the pore water is drained mostly through

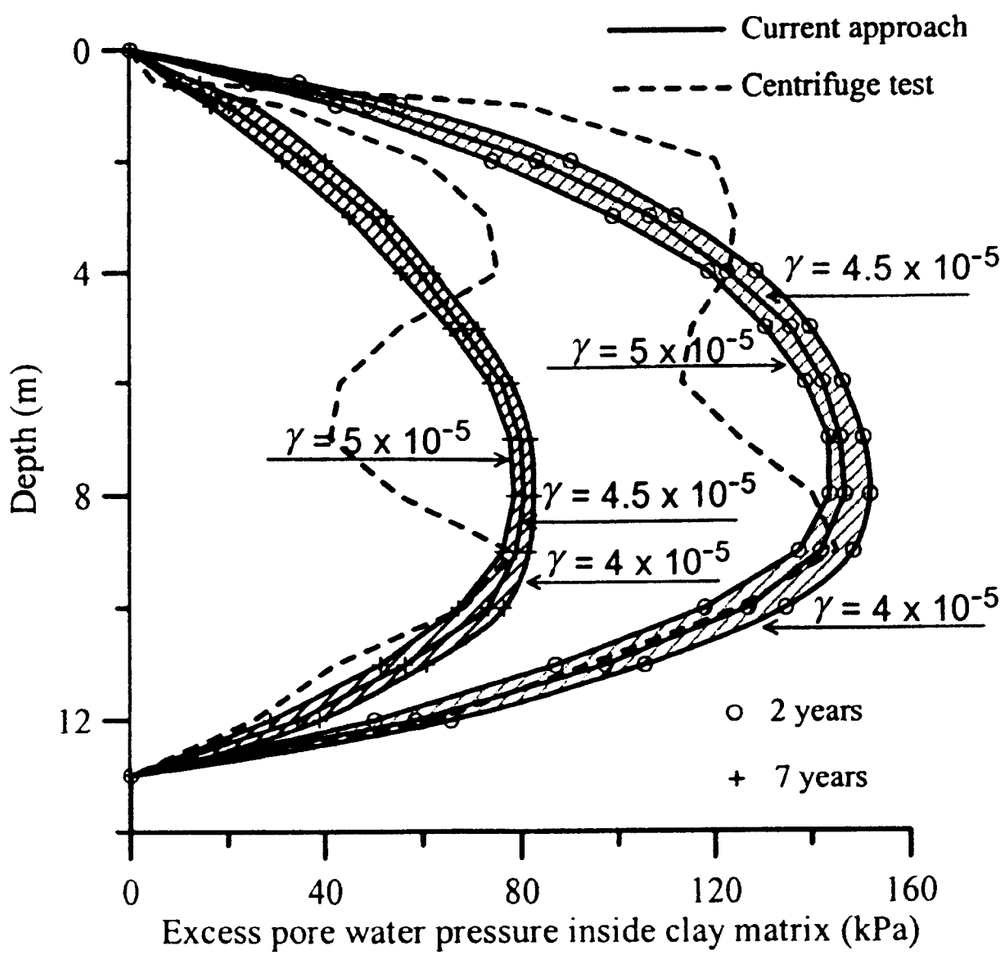

(a) Excess pore water pressure in clay matrix

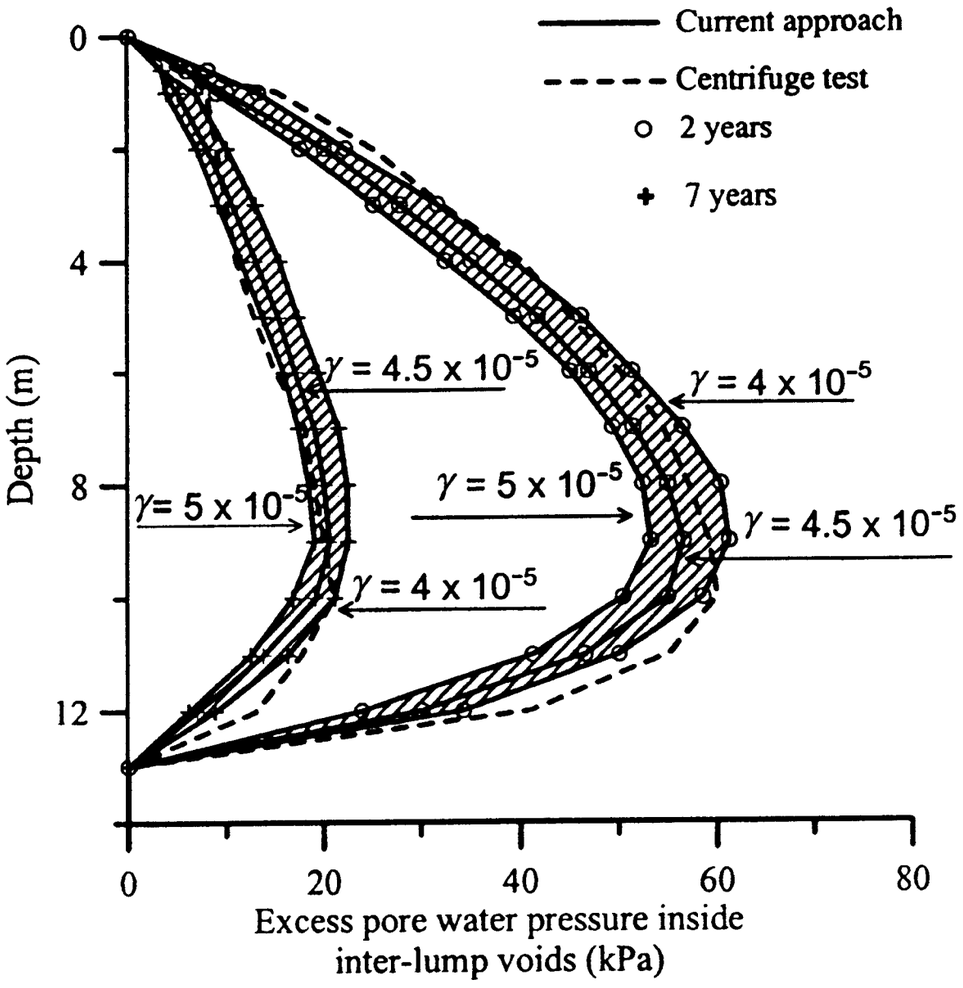

(b) Excess pore water pressure in inter-lump voids

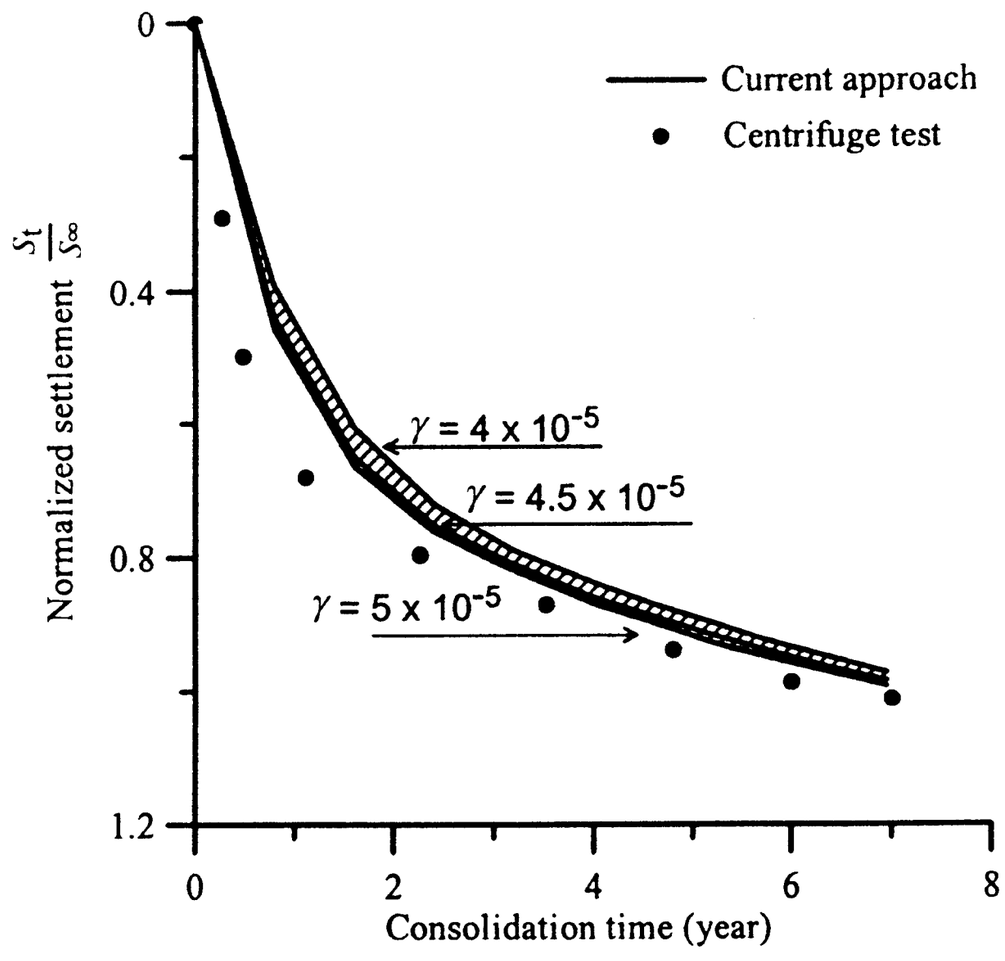

(c) Normalized settlement

Fig. 13. Comparison of test results and numerical results with Case 3 distribution of both m and $k_{(2)}$ along depth (test 2)

the matrix which results in a longer drainage path. On the other hand, a larger R_k implies higher permeability of inter-lump voids. Then, the pore water pressure in the inter-lump voids dissipates more quickly. After significant progress of drainage in inter-lump voids, these voids become good drainage paths for pore water in the matrix speeding up the consolidation process.

The effects of variation of $\delta_{(1)}$ are shown in Fig. 16. A more rapid consolidation rate is seen for smaller $\delta_{(1)}$ in the figure. This is because deformation of the matrix is more difficult for a smaller $\delta_{(1)}$. As a result, the fluid pressure dissipates relatively more through inter-lump voids than out of the matrix, which increases the consolidation rate as a whole.

The effects of variation of γ are shown in Fig. 17. It is observed that a longer consolidation time is required for smaller γ. This may be attributed to the fact that a higher fluid exchange rate between the matrix and inter-lump voids yields more rapid seepage of the fluid from the matrix into inter-lump voids and thus faster dissipation of pore pressure in lumpy clay fillings. Figure 18 shows the average degree of consolidation in matrix and inter-lump voids for two different γ. A shorter duration of stage II is observed for the higher fluid exchange factor as expected from the above argument.

Two Dimensional Consolidation Problem

A load is assumed to be applied on a limited area of the top surface as shown in Fig. 19. Only one particular set of the parameters ($\gamma = 1 \times 10^{-3}$, $R_k = 100$ and $\delta_{(1)} = 0.5$) is considered for this two-dimensional problem, in which the surface is assumed to be free-draining and the bottom is assumed to be rigid and imperious. Figure 20 shows the time histories of pore water pressure dissipations in matrix and inter-lump voids at the bottom of the fillings located at the center of the loaded area. The curves are similar to those observed in the one-dimensional consolidation problem and the consolidation process can still be divided into three distinct stages: stage I controlled by inter-lump voids; stage II controlled by both matrix and inter-lump voids; and stage III controlled by the matrix, which is characterized by the dominant dissipation of pore water pressure in the matrix since most of the pore water in the inter-lump voids has dissipated at stage III.

Figures 21 and 22 show respectively the distributions of excess pore water pressure along the vertical and horizontal planes at three different times. These planes are located respectively at the center of the loaded area and at

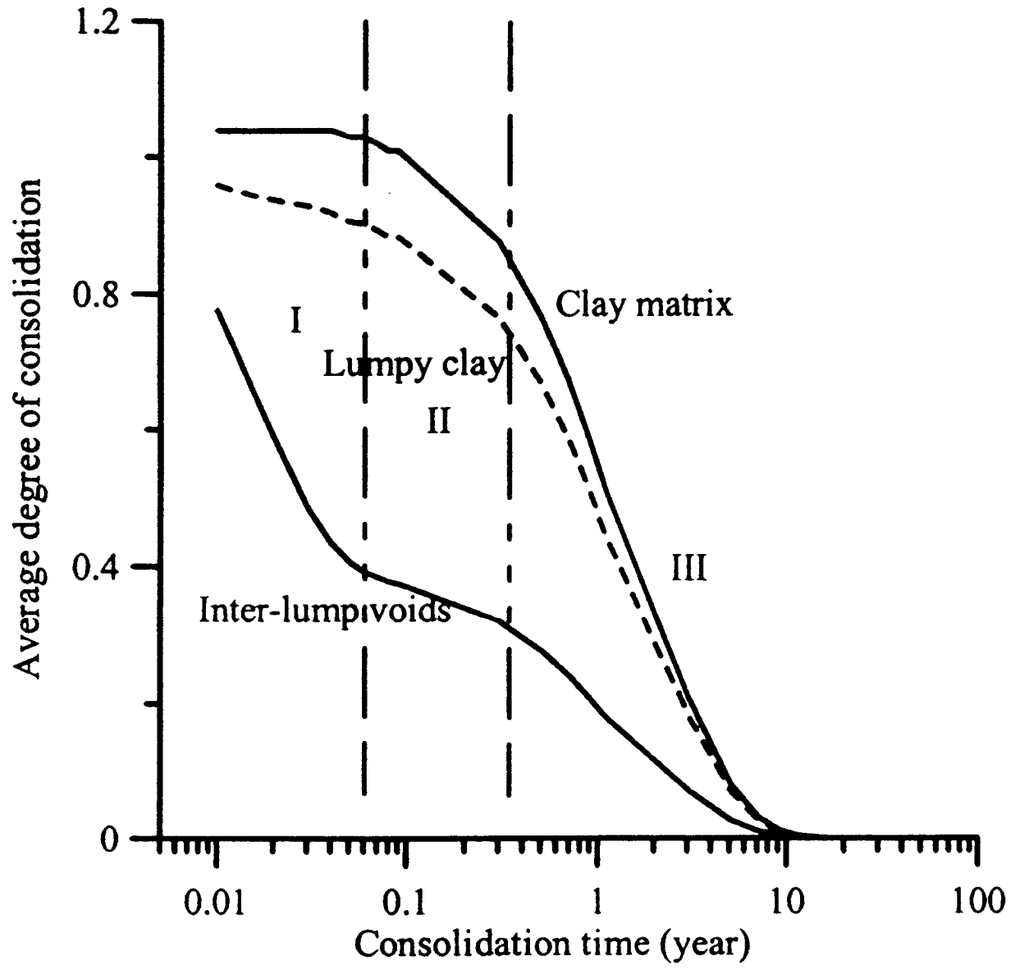

Fig. 14. Typical time-variations of average degrees of consolidation for clay matrix, inter-lump voids and overall system

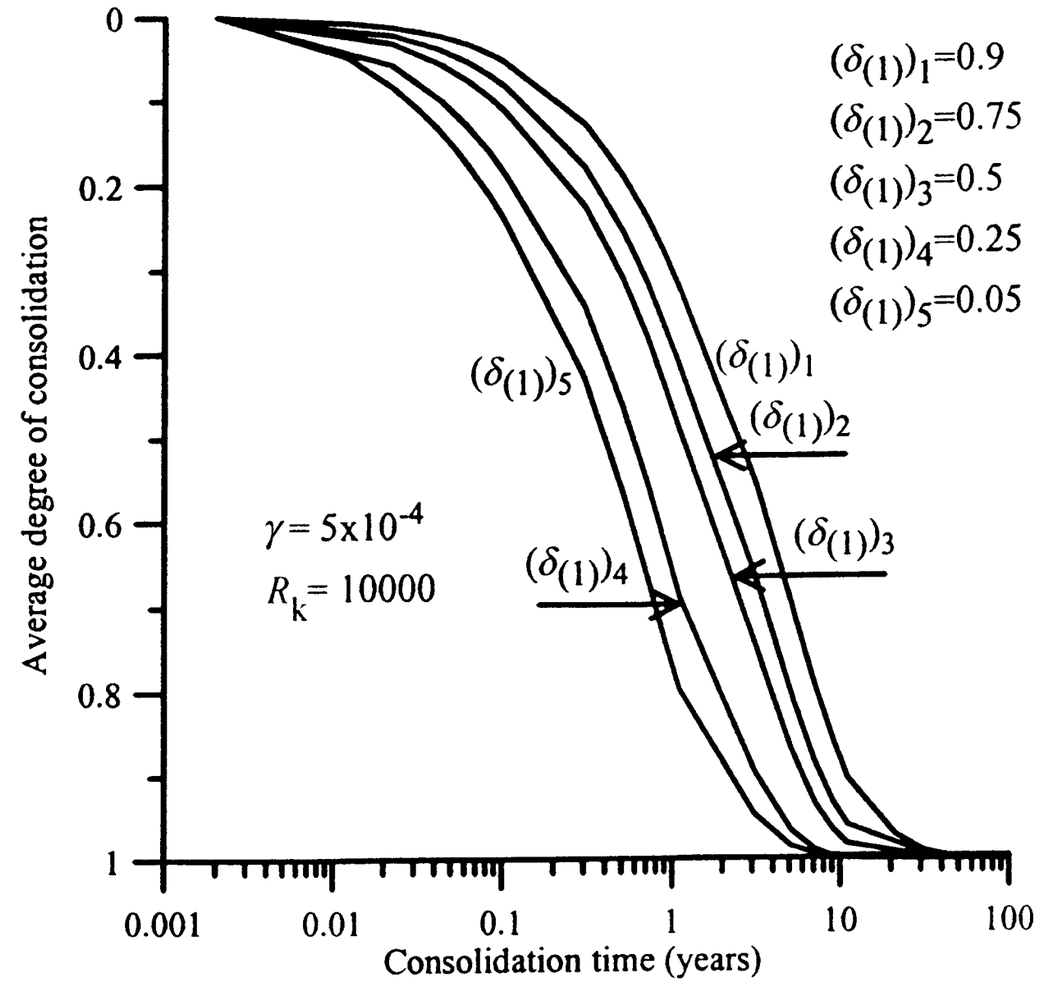

Fig. 16. Consolidation rate for different ratio of compressibility (δ_1)

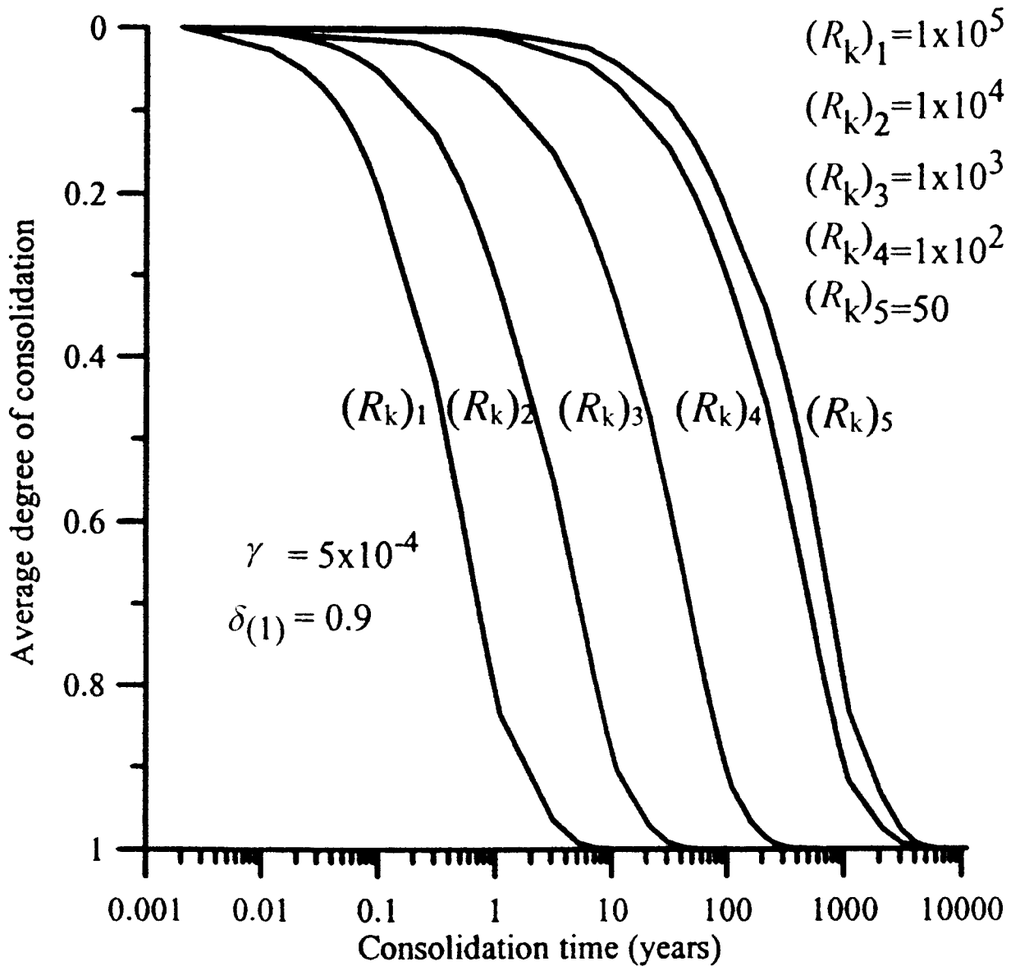

Fig. 15. Consolidation rate for different ratio of permeability (R_k)

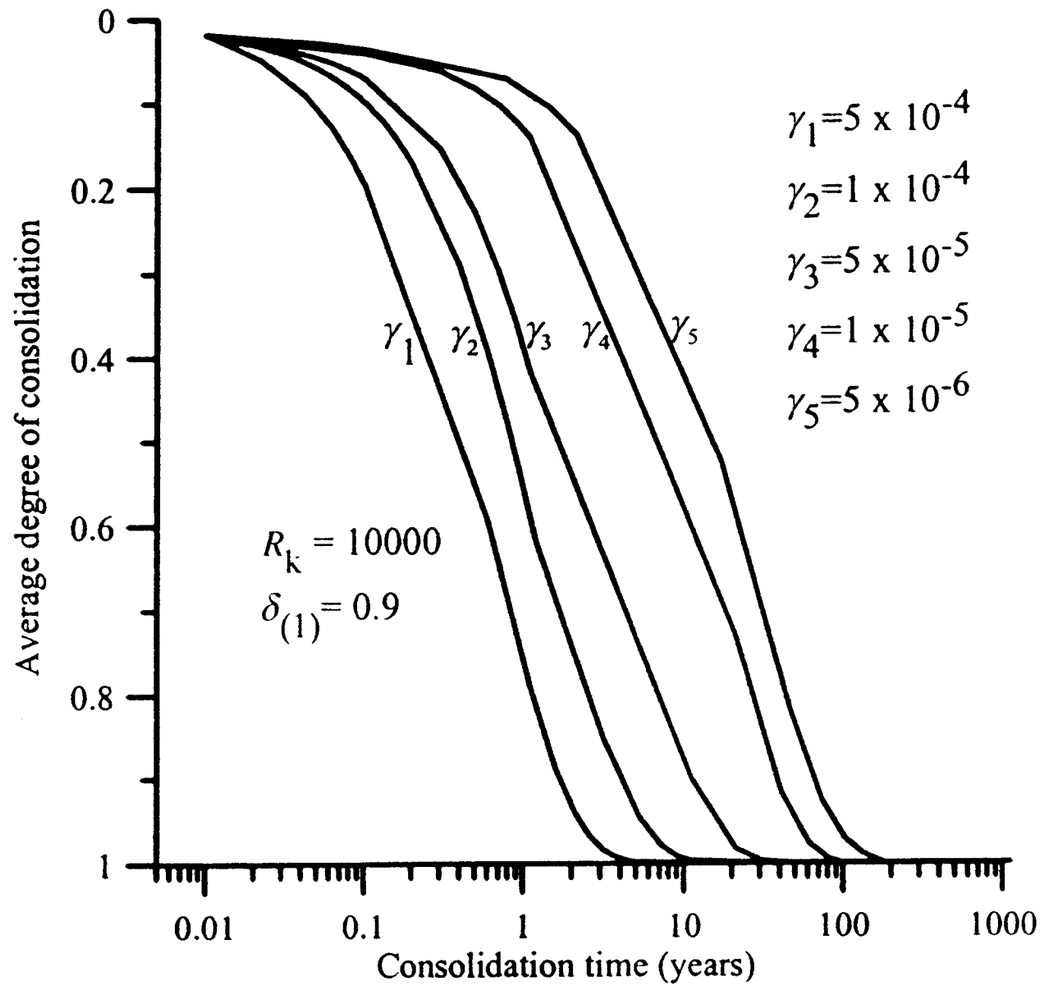

Fig. 17. Consolidation rate for different fluid exchange factor (γ)

1 m below the soil surface. The pore water pressure in the inter-lump voids dissipates faster than that in the clay matrix. Figure 23 shows vertical settlements of the layer. Due to the immediate settlement under the undrained condition (deformation without change in soil volume), the difference between the excess pore water pressures at $t=0.2$, 0.4 and 0.6 years is much larger than the difference between the settlements at these times. Figure 24 compares the consolidation behavior of clay as a single porosity soil and lumpy clay as a double porosity soil, for both the one-dimensional and two-dimensional conditions. The material properties of single porosity soil, which is assumed to possess a continuous distribution of a single type of void space satisfying a single permeability, are the same as those of the matrix in lumpy clay. It is seen that the effect of inter-lump voids on consolidation time is much more pronounced for the one-dimensional condition than for the two-dimensional condition.

CONCLUSIONS

A numerical method is developed for consolidation analysis of lumpy clay fillings by using the double porosity model and the meshless method. The developed method can consider: coupling of the deformation of soil

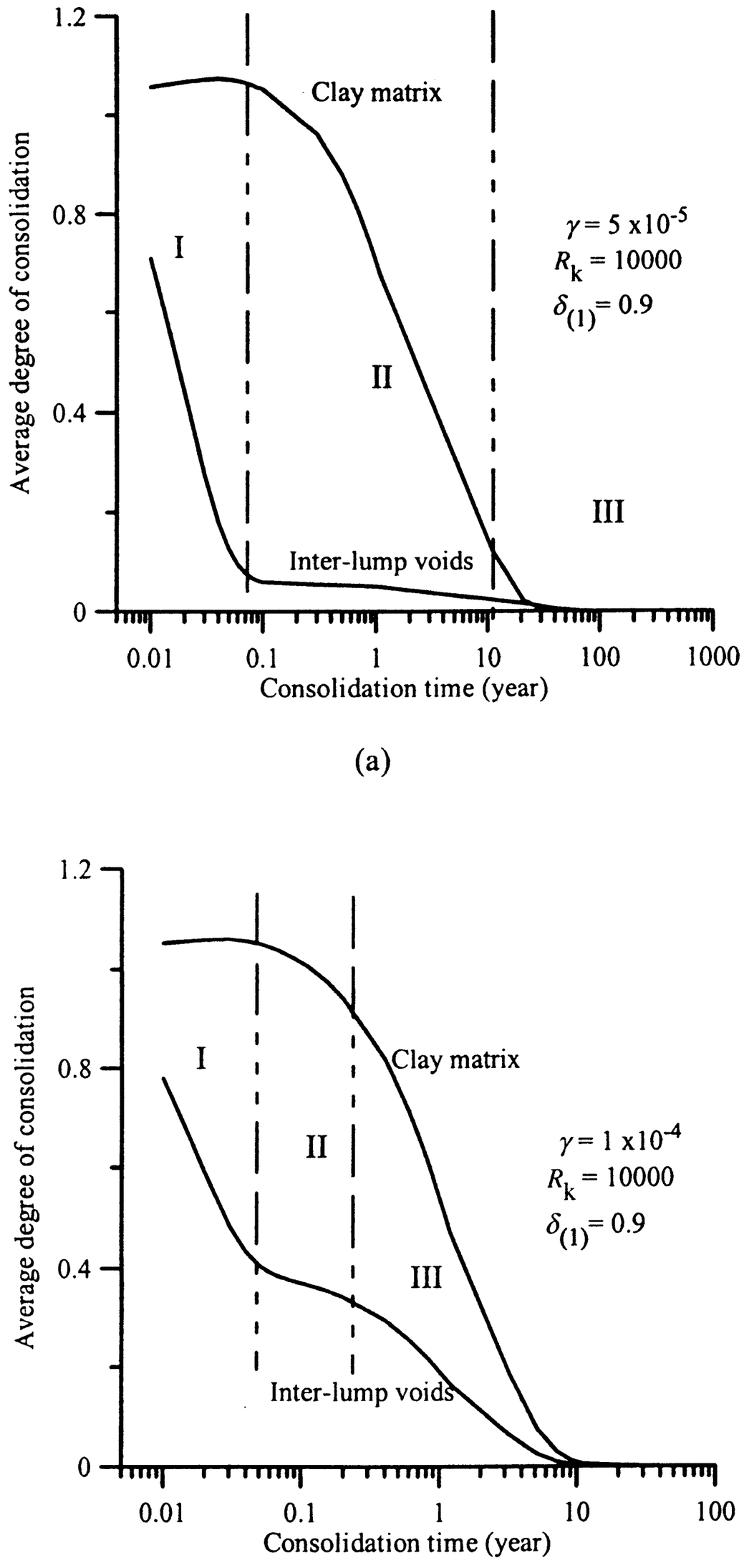

Fig. 18. Influence of fluid exchange factor on consolidation behavior

skeleton and the pore water pressures in both the clay matrix and inter-lump voids; and the fluid exchange between clay matrix and inter-lump voids. The pore water pressures and displacement are spatially discretized by using the Radial PIM meshless method with unequal-order interpolation functions. The developed method is verified through numerical results obtained by other methods and experimental results obtained by two centrifuge tests. Parameter studies are carried out for one-dimensional and two-dimensional problems. The following conclusions can be drawn from these studies:

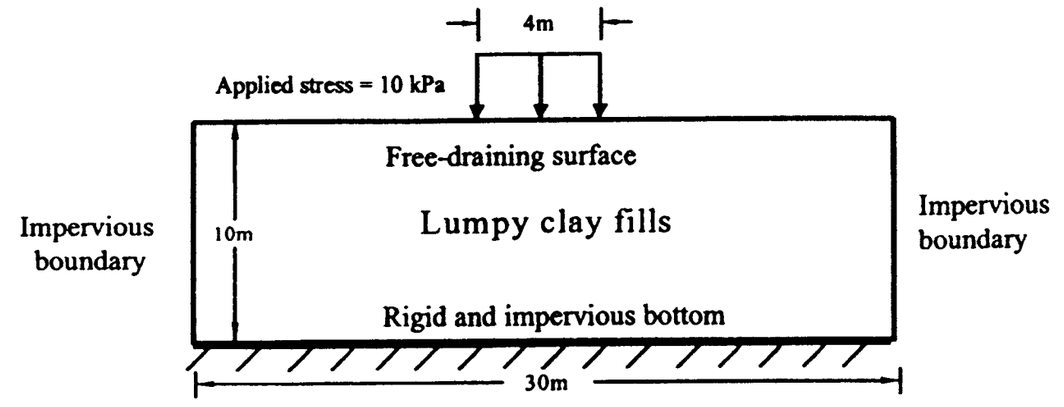

Fig. 19. Schematic description of a two-dimensional consolidation problem

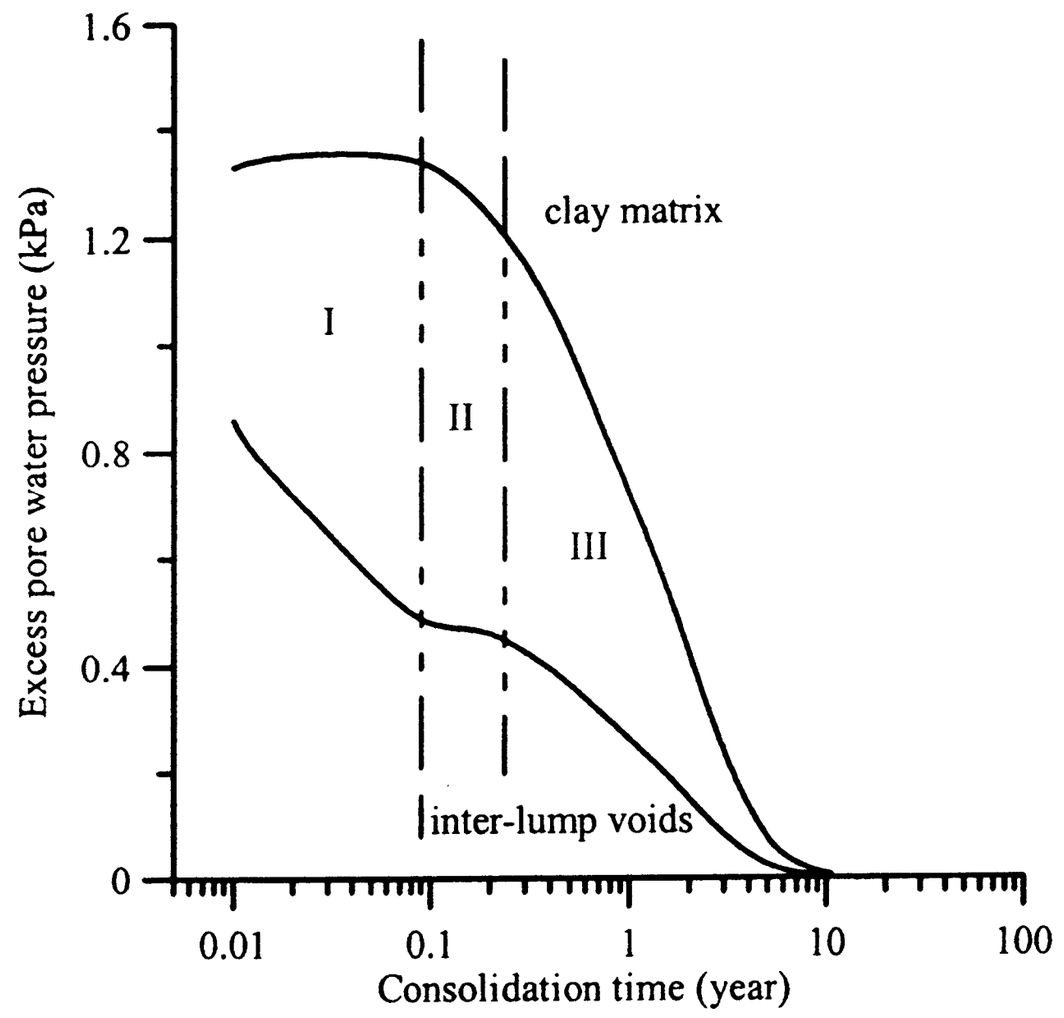

Fig. 20. Dissipation of excess pore water pressures in clay matrix and inter-lump voids at the base of the lumpy clay fillings located at the center of loaded area

(1) The double porosity model is well applicable for consolidation analysis of lumpy clay fillings. It is capable of taking into account the interaction between the deformation of soil skeleton and the pore water pressures in both the clay matrix and inter-lump voids, and also the fluid exchange between the matrix and inter-lump voids.
(2) The meshless method is effective for computation of consolidation behavior of lumpy clay fillings.
(3) The permeability ratio (R_k), compressibility ratio ($\delta_{(1)}$) and fluid exchange factor (γ) govern the consolidation process of lumpy clay fillings. The consolidation progresses faster for the higher permeability ratio, lower compressibility ratio and higher fluid exchange factor.
(4) The behaviours of pore water pressure dissipations are different in the clay matrix and inter-lump voids. When the permeability ratio is higher, the pore water pressure dissipates faster in inter-lump voids but slower in the matrix. When the compressibility ratio is lower, the pore water pressure dissipates

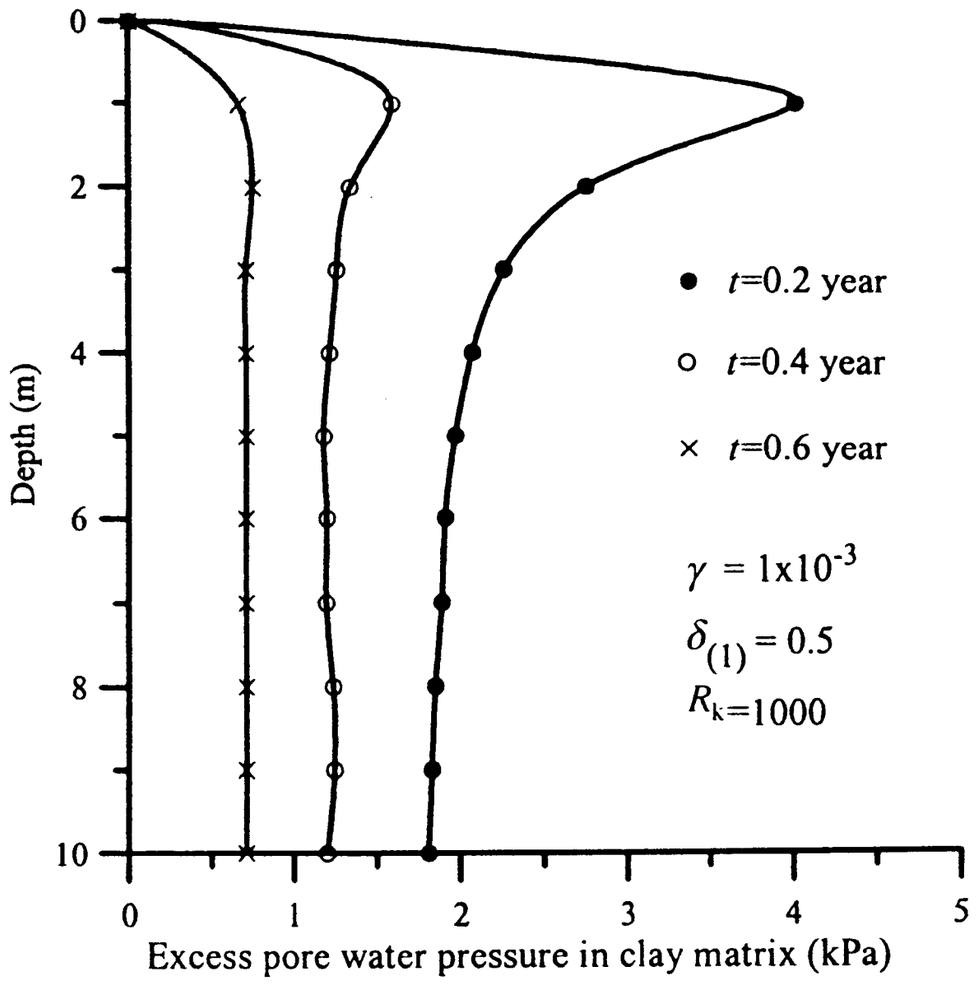

(a) Clay matrix

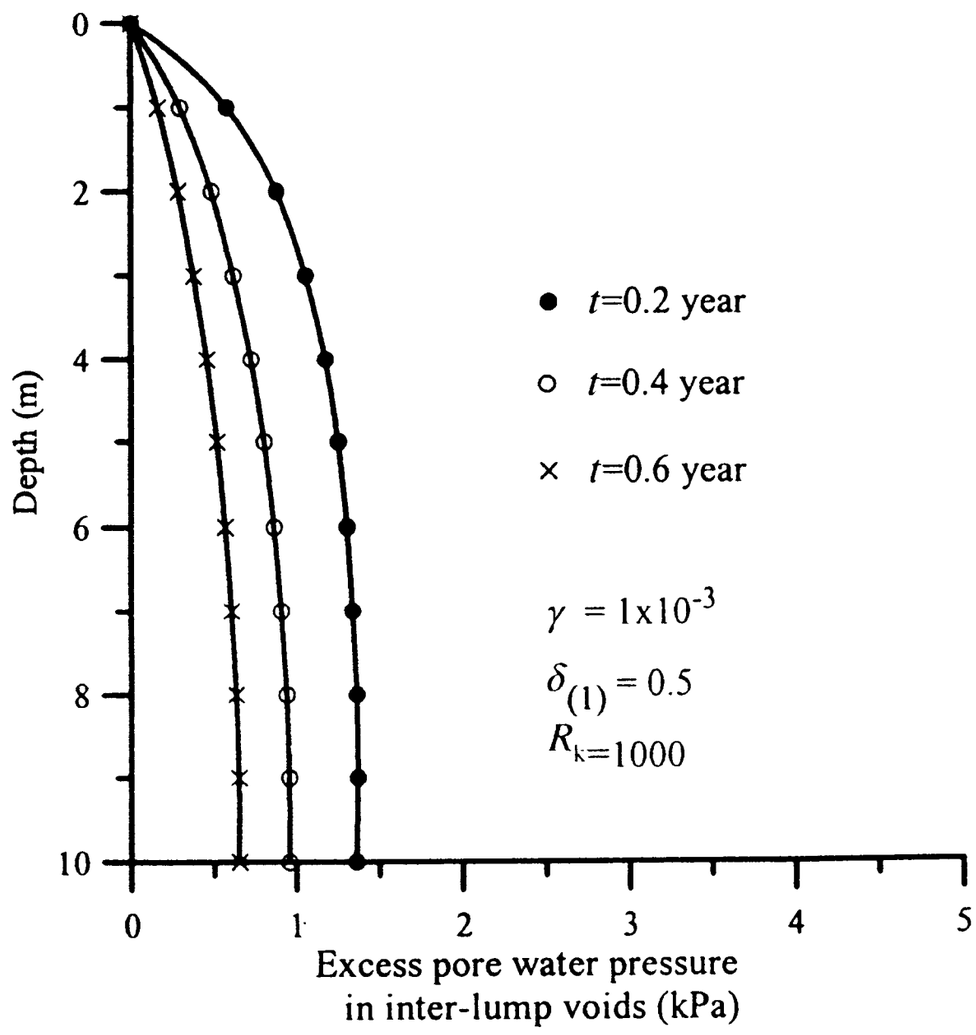

(b) Inter-lump voids

Fig. 21. Dissipation of pore water pressure along the depth at the center of loaded area at various times

slower in inter-lump voids but faster in the matrix. As the fluid exchange factor increases, the pore water pressure dissipates slower in inter-lump voids but faster in the matrix.

ACKNOWLEDGEMENT

The authors wish to acknowledge R. Manivanann for making the experimental results available for the present study.

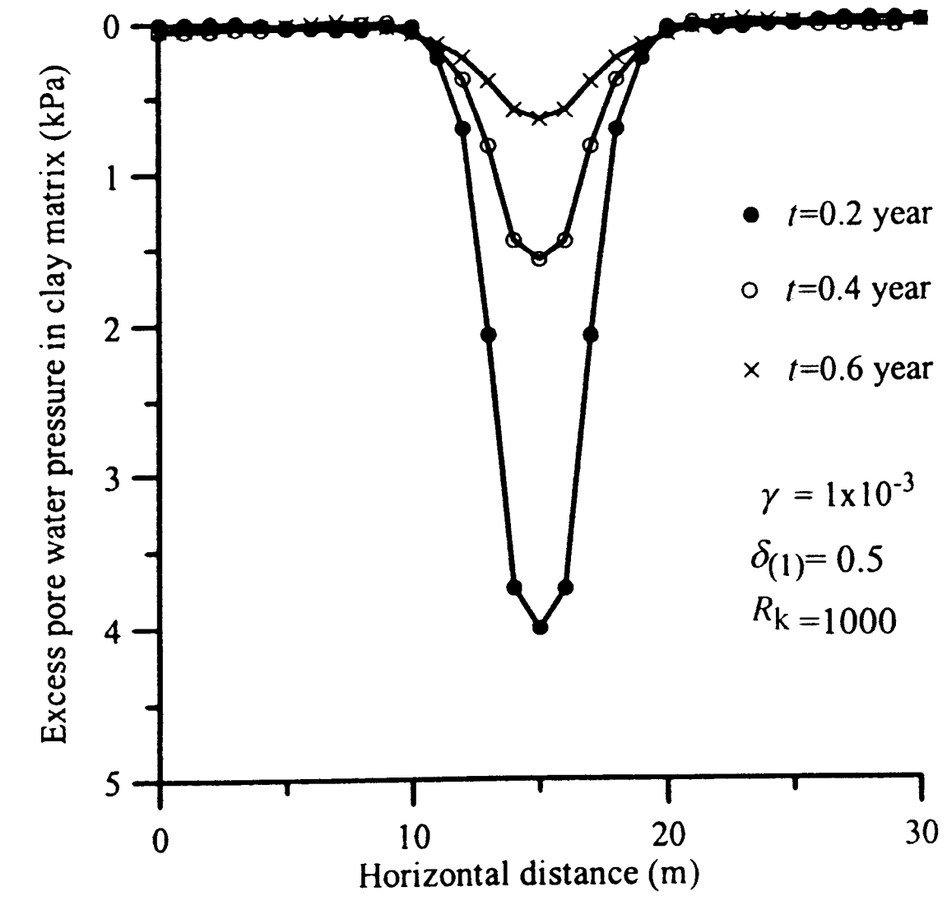

(a) Clay matrix

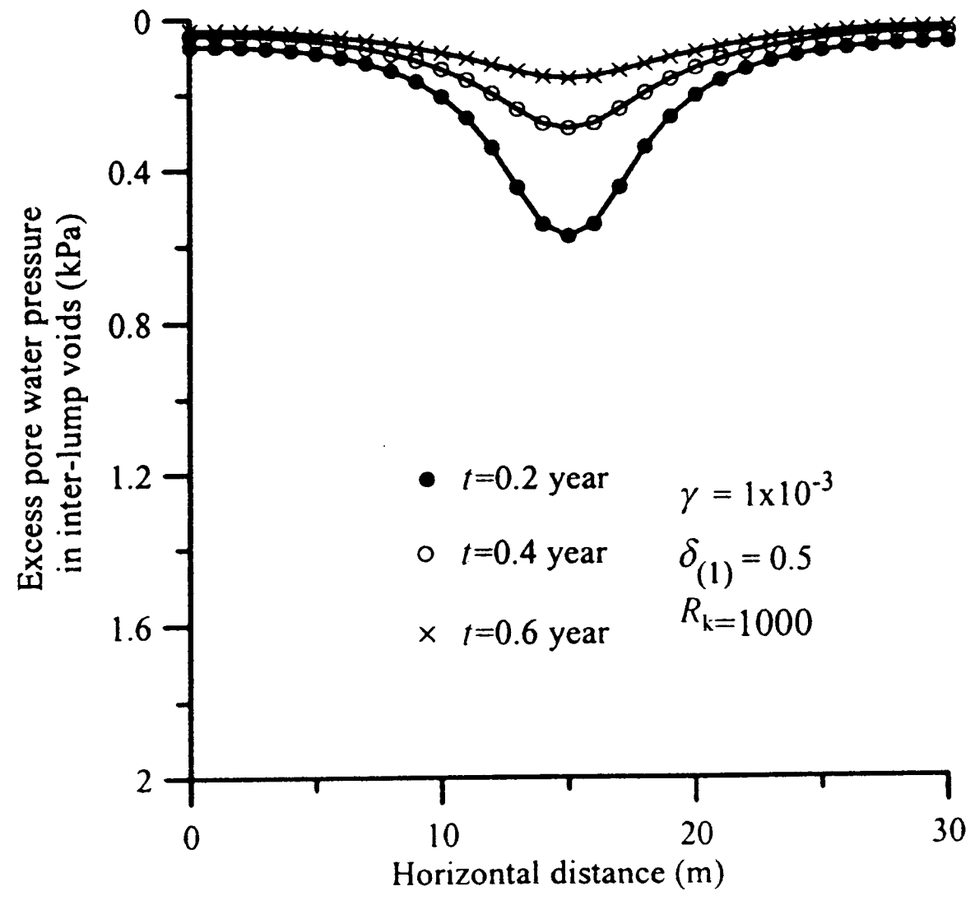

(b) Inter-lump voids

Fig. 22. Dissipation of pore water pressure along the horizontal plane 1 m below surface at various times

REFERENCES

1) Babuska, I. and Melenk, J. M. (1997): The partition of unity method, *Int. J. for Numerical Methods in Engrg.*, **40**, 727–758.
2) Bai, M. and Elsworth, D. (2001): Coupled process in subsurface deformation, flow, and transport, ASCE Press, Reston, VA, USA.
3) Bai, M., Ma, Q. and Roegiers, J. G. (1994): A nonlinear dual-porosity model, *Applied Mathematics Modelling*, **18**, 602–610.
4) Bai, M., Meng, F., Elsworth, D., Abousleiman, Y. and Roegiers, J. G. (1999): Numerical modeling of coupled flow and deformation in fractured rock specimens, *Int. J. for Numerical and Analytical Methods in Geomechanics*, **23**, 141–160.
5) Bai, M. and Roegiers, J. G. (1994): Dual-porosity behavior of naturally fractured reservoirs, *Int. J. for Numerical and Analytical Methods in Geomechanics*, **18**, 359–376.
6) Barenblatt, G. I., Zheltov, I. P. and Kochina, N. (1960): Basic concepts in the theory of seepage of homogeneous liquids in fissured

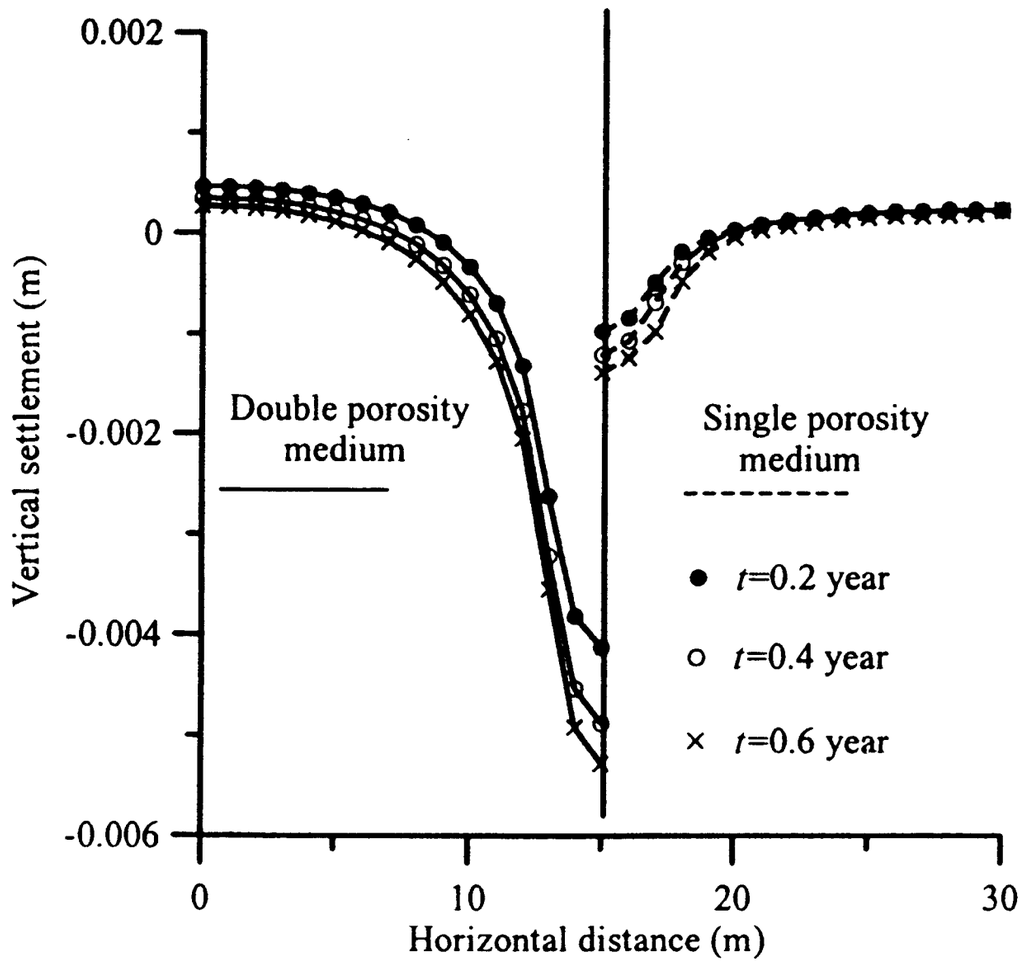

Fig. 23. Vertical settlement profile along the surface at various times

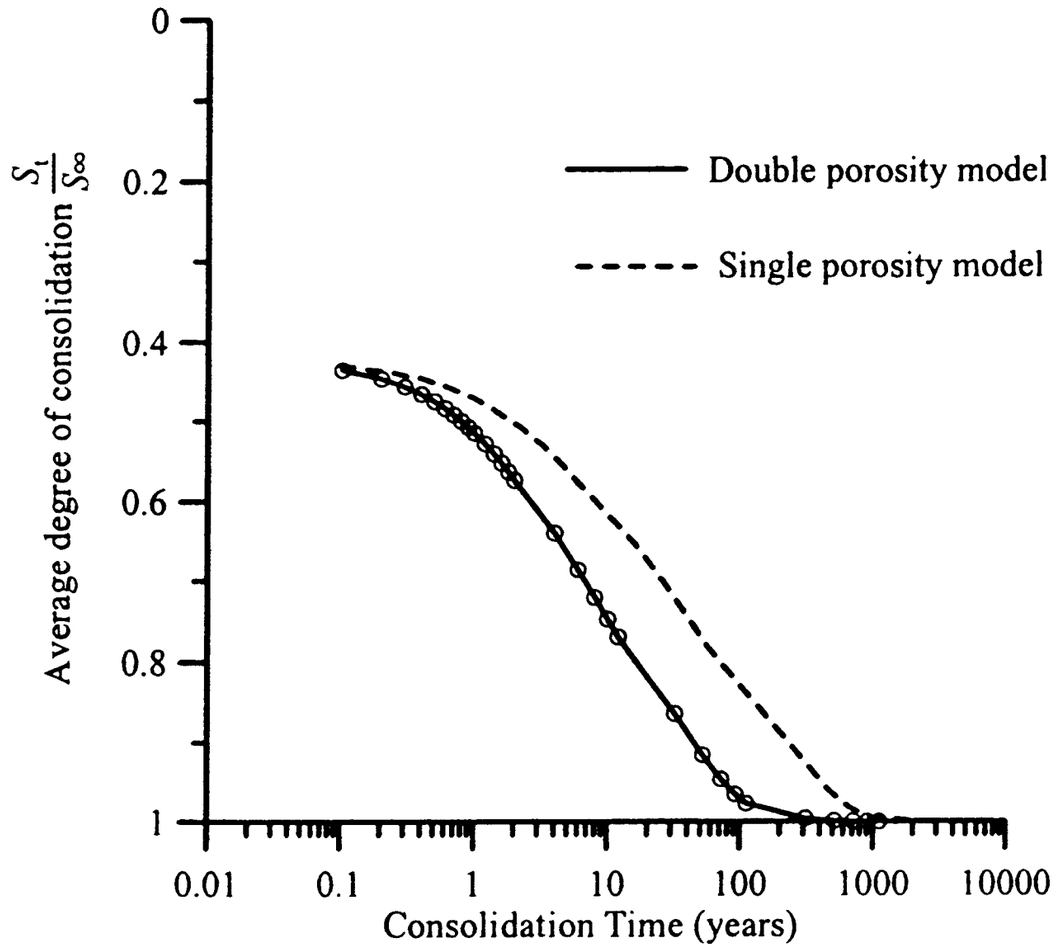

(a) Two-dimensional condition

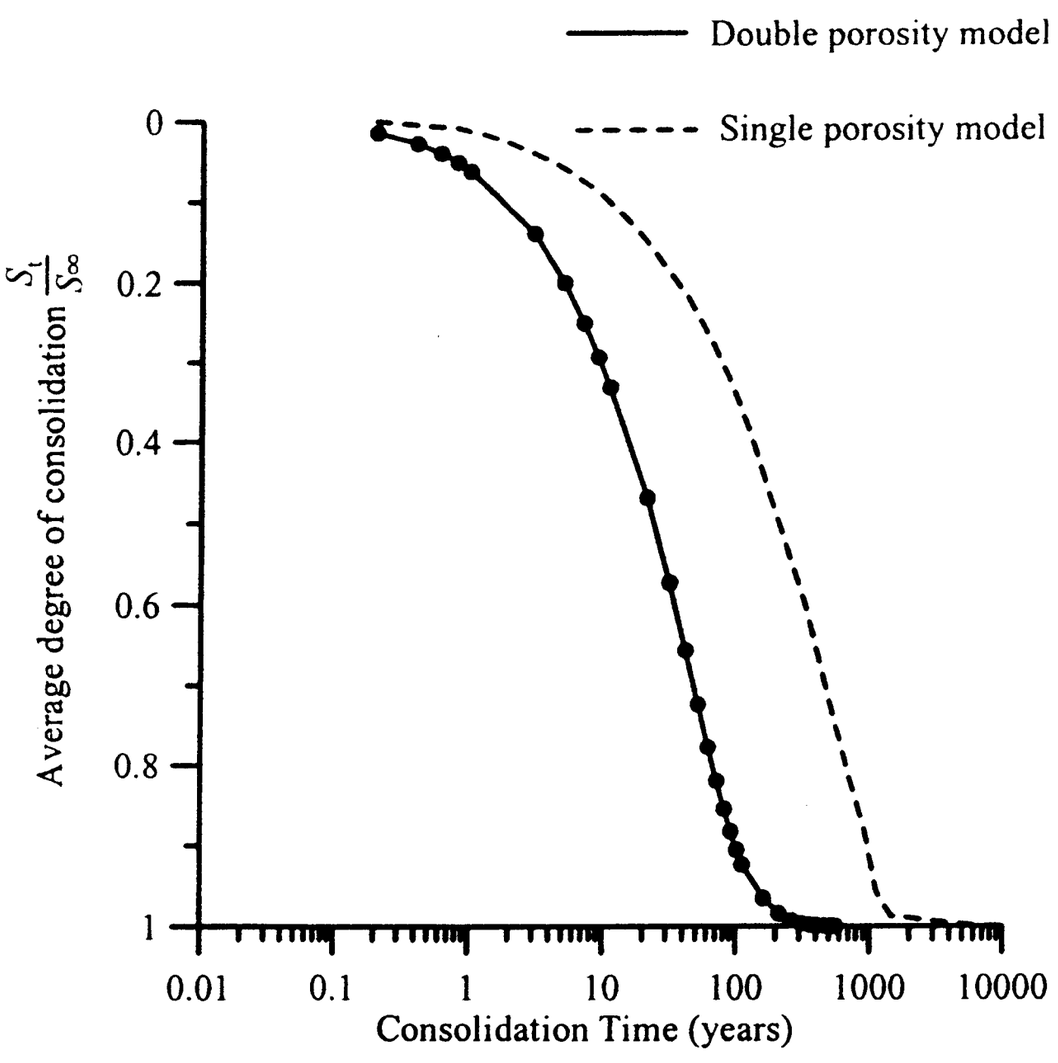

(b) One-dimensional condition

Fig. 24. Effects of double porosity on one-dimensional and two-dimensional consolidation behaviours

rocks, *J. of Applied Mathematics and Mechancis*, **24**, 1286–1303.
7) Bear, J. (1972): Dynamics of fluids in porous media, American Elsevier, New York.
8) Belytschko, T., Lu, Y. Y. and Gu, L. (1994): Element-free Galerkin methods, *Int. J. for Numerical Methods in Engrg.*, **37**, 229–256.
9) Berryman, J. G. and Wang, H. F. (1995): The elastic coefficients of double-porosity models for fluid transport in jointed rock, *J. of Geophysical Research*, **100**, 24611–24627.
10) Callari, C. and Federico, F. (2000): FEM validation of a double porosity elastic model for consolidation of structurally complex clayey soils, *Int. J. for Numerical and Analytical Method in Geomechanics*, **24**, 367–402.
11) Duarte, C. A. and Oden, J. T. (1996): Hp clouds-An h-p meshless method, *Numerical Methods for Partial Differential Equations*, **12**, 673–705.
12) Elsworth, D. and Bai, M. (1992): Flow-deformation response of dual-porosity media, *J. of. Geotech. Engrg.*, **118**, 107–124.
13) Ganesan, V. (1998): Layered clay-sand scheme of land reclamation, *Ph.D thesis*, National Univ. of Singapore.
14) Ghafouri, H. R. and Lewis, R. W. (1996): A finite element double porosity model for heterogeneous deformable porous media, *Int. J. for Numerical and Analytical Method in Geomechanics*, **20**, 831–844.
15) Hartlen, J. and Inters, C. (1981): Land reclamation using fine-grained dredged material, *Proc. 10th Int. Conf. on Soil Mechanics and Foundation Engrg.*, Stockholm, 145–148.
16) Khalili, N. and Valliappan, S. (1995): Fissured clay consolidation: a mathematical model, *Proc. Int. Symp. on Compression and Consolidation of Clayey Soils*, Hiroshima, Japan, 10–12.
17) Khalili, N., Valliappan, S. and Wang, C. F. (1999): Consolidation of fissured clays, *Géotechnique*, **49**, 75–89.
18) Lee, F. H., Tan, T. S., Leung, C. F., Yong, K. Y., Karunaratne, G. P. and Lee, S. L. (1991): Development of geotechnical centrifuge facility at the National University of Singapore, *Proc. Int. Conf. Centrifuge 91*, Ko and McLean, Rotterdam, Holland, 11–17.
19) Leung, C. F., Lau, A. H., Wong, J. C. and Karunaratne, G. P. (1996): Centrifuge model tests of dredged material, *Proc. 2nd Int. Conf. on Soft Soil Engrg.*, NanJing, China, **1**, 401–406.
20) Leung, C. F., Wong, J. C., Manivanann, R. and Tan, S. A. (2001): Experimental evaluation of consolidation behavior of stiff clay lumps in reclamation fill, *Geotech. Testing J.*, **24** (2), 145–156.
21) Lewallen, K. T. and Wang, H. F. (1998): Consolidation of a double-porosity medium, *Int. J. of Solids Structures*, **35**, 4845–4867.
22) Li, M. (2001): Consolidation of clay with permeable elements, *Master thesis*, National Univ. of Singapore.
23) Liu, W. K., Jun, S. and Zhang, Y. F. (1995): Reproducing kernel particle methods, *Int. J. for Numerical Methods in Fluids*, **20**, 1081–1106.
24) Lucy, L. B. (1977): A numerical approach to the testing of the fission hypothesis, *The Astronomical J.*, 1013–1024.
25) Mannivanann, R. (1999): Land reclamation using dredged materials, *Research Proposal for Ph.D. Pre-Exam*, National Univ. of Singapore.
26) Modaressi, H. and Aubert, P. (1996): A diffuse element-finite element technique for transient coupled analysis, *Int. J. for*

Numerical Methods in Engrg., **39**, 3809–3838.
27) Murakami, A., Kawabata, H. and Aoyama, S. (2001): EFGM analysis for saturated soil, *Computer Methods and Advances in Geomechanics* (eds. by Desai et al.), **1**, 153–156.
28) Nayroles, B., Touzot, G. and Villon, P. (1992) Generalizing the finite element method: diffuse approximation and diffuse elements, *Computational Mechanics*, **10**, 307–318.
29) Nogami, T., Wang, W. and Li, M. (2001): Consolidation of lumpy clay fills, *Proc. Computational Mechanics—New Frontiers for New Millennium, 1st Asian-Pacific Congress on Computational Mechanics*, Sydney, Australia.
30) Nur, A. and Byerlee, J. D. (1971): An exact effective stress law for elastic deformation of rock with fluids, *J. of Geophysical Research*, **76**, 6414–6419.
31) Valliappan, S. and Khalili, N. (1990): Flow through fissured porous media with deformable matrix, *Int. J. for Numerical Methods in Engrg.*, **29**, 1074–1094.
32) Wang, J. G., Leung, C. F. and Chow, Y. K. (1997): Consolidation analysis of lumpy fills using a homogenization method, *Proc. 9th Int. Conf. on Computer Method and Advanced Geomechanics*, 1075–1080.
33) Wang, J. G. and Liu, G. R. (2002): A point interpolation meshless method based on radial basis functions, *Int. J. for Numerical Methods in Engrg.*, **54**, 1014–1201.
34) Wang, J. G. and Liu, G. R. (2002): A point interpolation meshless method based on radial basis functions, *Int. J. for Numerical Methods in Engrg.*, **54**, 1623–1648.
35) Wang, J. G., Liu, G. R. and Lin, P. (2002): Numerical analysis of Biot's consolidation process by radial point interpolation method, *Int. J. of Solids and Structures*, **39**, 1557–1573.
36) Wang, J. G., Liu, G. R. and Wu, Y. G. (2001): A point interpolation method for simulating dissipation process of consolidation, *Computer Methods in Applied Mechanics and Engrg.*, **190**, 5907–5922.
37) Warren, J. E. and Root, P. J. (1963): The behavior of naturally fractured reservoirs, *Transactions*, AIME., **23**, 245–255.
38) Wilson, R. K. and Aifantis, E. C. (1982): On the theory of consolidation with double porosity, *Int. J. of Engrg. Science*, **20**, 1009–1035.
39) Wong, J. C. (1997): Model studies of lumpy fill, *Master Thesis*, National Univ. of Singapore.

APPENDIX A: RADIAL POINT INTERPOLATION METHOD

Consider an approximation function $u(\boldsymbol{x})$ in the influence domain. This function has a set of arbitrarily distributed points $P_i(\boldsymbol{x}_i)$ $(i=1, 2, \cdots, n)$ within the influence domain. n is the number of nodes. The function has value u_i at each node point $\boldsymbol{x}_i$. The radial PIM method constructs the $u(\boldsymbol{x})$ through a linear combination of radial basis $B_i(\boldsymbol{x})$ and polynomial basis $p_j(\boldsymbol{x})$:

$$u(\boldsymbol{x})=\sum_{i=1}^{n} B_i(\boldsymbol{x})a_i+\sum_{j=1}^{m} P_j(\boldsymbol{x})b_j=\boldsymbol{B}^T(\boldsymbol{x})\boldsymbol{a}+\boldsymbol{P}^T(\boldsymbol{x})\boldsymbol{b} \tag{24}$$

where a_i is the coefficient for $B_i(\boldsymbol{x})$ and b_j the coefficient for $p_i(\boldsymbol{x})$ (usually, $m<n$). The vectors are defined as

$$\begin{aligned}
&\boldsymbol{a}^T=[a_1 a_2 a_3 \cdots a_n]\\
&\boldsymbol{b}^T=[b_1 b_2 \cdots b_m]\\
&\boldsymbol{B}^T(\boldsymbol{x})=[B_1(\boldsymbol{x})\,B_2(\boldsymbol{x})\,B_3(\boldsymbol{x})\cdots B_n(\boldsymbol{x})]\\
&\boldsymbol{P}^T(\boldsymbol{x})=[p_1(\boldsymbol{x})\,p_2(\boldsymbol{x})\cdots p_m(\boldsymbol{x})]
\end{aligned} \tag{25}$$

Generally, the $B_i(\boldsymbol{x})$ has the following form for a two-dimensional problem

$$\begin{aligned}
B_i(\mathbf{x})&=B_i(r_i)=B_i(x, y)\\
r_i&=[(x-x_i)^2+(y-y_i)^2]^{1/2}
\end{aligned} \tag{26}$$

Polynomial basis functions have following monomial terms:

$$\boldsymbol{P}^T(\boldsymbol{x})=[1\ x\ y\ x^2\ xy\ y^2\cdots] \tag{27}$$

The coefficients a_i and b_j in Eq. (24) are determined by enforcing the $u(\mathbf{x})$ to pass through all n scattered points:

$$u_k=u(x_k, y_k)=\sum_{i=1}^{n} a_i B_i(x_k, y_k)+\sum_{j=1}^{m} b_j P_j(x_k, y_k)$$
$$k=1, 2, \cdots, n \tag{28}$$

A constraint is necessary to insure that the approximation is unique:

$$\sum_{i=1}^{n} P_j(x_i, y_i)a_i=0 \quad j=1, 2, \cdots, n \tag{29}$$

It is expressed in matrix form as follows

$$\begin{bmatrix} \boldsymbol{B}_0 & \boldsymbol{P}_0 \\ \boldsymbol{P}_0^T & \boldsymbol{0} \end{bmatrix} \begin{Bmatrix} \boldsymbol{a} \\ \boldsymbol{b} \end{Bmatrix} = \begin{Bmatrix} \boldsymbol{u}^e \\ \boldsymbol{0} \end{Bmatrix} \quad \text{or} \quad \boldsymbol{G}=\begin{Bmatrix} \boldsymbol{a} \\ \boldsymbol{b} \end{Bmatrix} = \begin{Bmatrix} \boldsymbol{u}^e \\ \boldsymbol{0} \end{Bmatrix} \tag{30}$$

where the vector for function values at each node is

$$\boldsymbol{u}^e=[u_1\ u_2\ u_3\cdots u_n]^T \tag{31}$$

The coefficient matrix $\boldsymbol{B}_0$ on unknowns $\boldsymbol{a}$ is

$$\boldsymbol{B}_0=\begin{bmatrix} B_1(x_1, y_1) & B_2(x_1, y_1) & \cdots & B_n(x_1, y_1) \\ B_1(x_2, y_2) & B_2(x_2, y_2) & \cdots & B_n(x_2, y_2) \\ \vdots & \vdots & \vdots & \vdots \\ B_1(x_n, y_n) & B_2(x_n, y_n) & \cdots & B_n(x_n, y_n) \end{bmatrix}_{n\times n} \tag{32}$$

The coefficient matrix $\boldsymbol{P}_0$ on unknowns $\boldsymbol{b}$ is

$$\boldsymbol{P}_0=\begin{bmatrix} P_1(x_1, y_1) & P_2(x_1, y_1) & \cdots & P_m(x_1, y_1) \\ P_1(x_2, y_2) & P_2(x_2, y_2) & \cdots & P_m(x_2, y_2) \\ \vdots & \vdots & \vdots & \vdots \\ P_1(x_n, y_n) & P_2(x_n, y_n) & \cdots & P_m(x_n, y_n) \end{bmatrix}_{n\times m} \tag{33}$$

The solution is obtained if the inverse of matrix $\boldsymbol{G}$ or $\boldsymbol{B}_0$ exists:

$$\begin{Bmatrix} \boldsymbol{a} \\ \boldsymbol{b} \end{Bmatrix} = \boldsymbol{G}^{-1} \begin{Bmatrix} \boldsymbol{u}^e \\ \boldsymbol{0} \end{Bmatrix} \tag{34}$$

The interpolation is finally expressed as

$$u(\boldsymbol{x})=[\boldsymbol{B}^T(\boldsymbol{x})\boldsymbol{P}^T(\boldsymbol{x})]\boldsymbol{G}^{-1}=\begin{Bmatrix} \boldsymbol{u}^e \\ \boldsymbol{0} \end{Bmatrix}=\boldsymbol{\phi}(\boldsymbol{x})\boldsymbol{u}^e \tag{35}$$

where the matrix of shape functions $\boldsymbol{\phi}(\boldsymbol{x})$ is defined by

$$\begin{aligned}
\boldsymbol{\phi}(\boldsymbol{x})&=[\phi_1(\boldsymbol{x})\phi_2(\boldsymbol{x})\cdots\phi_i(\boldsymbol{x})\cdots\phi_n(\boldsymbol{x})]\\
\phi_k(\boldsymbol{x})&=\sum_{i=1}^{n} B_i(\boldsymbol{x})\bar{G}_{i,k}+\sum_{j=1}^{m} P_j(\boldsymbol{x})\bar{G}_{n+j,k}
\end{aligned} \tag{36}$$

where $\bar{G}_{i,k}$ is the (i, k) element of matrix $\boldsymbol{G}^{-1}$. The derivatives of shape functions are

$$\frac{\partial \phi_k}{\partial x} = \sum_{i=1}^{n} \frac{\partial B_i}{\partial x} \bar{G}_{i,k} + \sum_{j=1}^{m} \frac{\partial P_j}{\partial x} \bar{G}_{n+j,k}$$
$$\frac{\partial \phi_k}{\partial y} = \sum_{i=1}^{n} \frac{\partial B_i}{\partial y} \bar{G}_{i,k} + \sum_{j=1}^{m} \frac{\partial P_j}{\partial y} \bar{G}_{n+j,k} \quad (37)$$

Gaussian type radial functions are widely used in mathematics:

$$B_i(x, y) = \exp(-br_i^2) \quad (38)$$

where $b(b \geq 0)$ is a shape parameter. The partial derivatives are again obtained as follows

$$\frac{\partial B_i}{\partial x} = -2bB_i(x, y)(x - x_i)$$
$$\frac{\partial B_i}{\partial y} = -2bB_i(x, y)(y - y_i) \quad (39)$$

APPENDIX B: UNEQUAL ORDER APPROXIMATION FOR RADIAL PIM

The radial PIM constructs the interpolation function through a linear combination of the radial basis and polynominal basis in the above expressions. The order of interpolation function referred to in this paper is the order of the polynominal base that is associated with P_j. When the order is higher, the term m in the summation sign in the polynominal basis portion is larger. The unequal order approximation is used for the finite element method, but it is new to the meshless method. The effect of the unequal order approximation approach on the computational results is examined. A typical one-dimensional problem shown in Fig. 5(a) and a regular node distribution are adopted. Material constants used in the computation are $E = 10$ MPa, $\nu = 0$, $k_{(1)} = 1 \times 10^{-4}$ m/year, $k_{(2)} = 1 \times 10^{-1}$ m/year, $n_{(2)} = 0.1$, and $\gamma = 1 \times 10^{-4}$. Table A shows the relative error distribution of pore water pressure inside the clay matrix and inter-lump voids with depth under the equal approximation scheme and unequal approximation. The relative error is defined as:

$$\varepsilon_u = \frac{p^{PIM} - p^{FEM}}{p^{FEM}} \times 100(\%)$$

where p^{FEM} and p^{PIM} mean the excess pore water pressure computed from the FEM and radial PIM respectively. From the table, it is shown that the unequal approximation scheme has less relative error than the equal approximation scheme (the conventional radial PIM) and thus is of higher accuracy.

Table A. Relative error distribution of pore water pressure inside the clay matrix and inter-lump voids with depth under the equal approximation scheme and unequal approximation

Depth (m)	Equal order approximation		Unequal order approximation	
	Pore water pressure inside clay matrix	Pore water pressure inside inter-lump voids	Pore water pressure inside clay matrix	Pore water pressure inside inter-lump voids
0	0	0	0	0
2	−4.56	−5.32	−3.42	−5.01
4	−5.21	−6.22	−5.02	−4.89
6	−4.11	4.17	−3.88	3.75
8	3.21	−3.22	−2.12	−2.01
10	−5.83	−4.22	−3.74	1.27